2020（令和2）年度　　修士学位論文

再結晶缶を用いたスラリーアイスの
氷粒子径コントロールに関する研究

Study on control of ice particle size in slurry ice by utilizing recrystallizer module

2020 年 9 月 9 日

高知工科大学大学院　　工学研究科基盤工学専攻
知能機械システム工学コース

1227001　　Kanin NGAMRUNGKIJ

指導教員　　　松本　泰典

Academic Year 2020

Master's Thesis

Study on control of ice particle size in slurry ice by utilizing recrystallizer module

1227001   Kanin NGAMRUNGKIJ

Advisor   *Assoc. Prof.* Matsumoto Yasunori

9th September, 2020

Intelligent Mechanical Engineering course

Graduate School of Engineering

Kochi University of Technology

Abstract

Study on control of ice particle size in slurry ice
by utilizing recrystallizer module.

Kanin NGAMRUNGKIJ

Freeze concentration is a process used to increase the overall concentration of liquid food by partially freezing the water content into ice particles forming a slurry of ice particles and the solution. The ice particles were then removed from the product by a centrifugal machine. This process proved useful in maintaining the distinctive aromas and flavor of liquid food which is susceptible to heat degradation such as fruit juices and dairy products. To give the ice particles time to grow and to make controlling possible a recrystallizer module was utilized. In this module agitation is essential in preventing the ice particles from coagulation and causing the fluid pumping to come to a halt.

This research studies on (1) the agitation effects on ice particles growth characteristics within the recrystallizer module (2) mechanisms involved, heavily focuses on the Ostwald ripening, and (3) the correlation of time and ice particle growth rate.

Table of Contents

List of Figures

List of Tables

Chapter 1: Introduction

In the food industries, freeze concentration was used to increase the concentration of liquid food while maintaining its characteristic aromas and flavors that is susceptible to heat degradation [1]. This process partially freezes the water contents in the liquid into ice particles of pure water. The slurry consisting of ice particles and the product were then separated in a centrifugal machine giving a much more concentrated product. In doing this there tends to be some residue liquid attached to the surface of the ice particles, the smaller the ice particles the more liquid is loss through this process and vice versa. To give the ice particles time to grow and to make controlling possible a recrystallizer module is utilized. In this module agitation is essential in preventing the ice particles from coagulation and causing the fluid pumping to come to a halt.

This research studies on the agitation effects on ice particles growth characteristics within the recrystallizer module and mechanisms involved with a heavy emphasis on the Ostwald ripening mechanism.

Chapter 2: Background study

This chapter will be discussing about the background and studies related to this research.

2.1 Food processing

Food processing is any method that transform produce into edible product. The whole process maybe only a single or multiple step such as washing, cooking, concentrating, and many more. Food processing doesn't strictly limit to primary processing of transforming raw produce into edible product. Secondary processing of turning edible product into other product such as turning orange juice into orange-flavored popsicle is included as well.

As the food industry grows larger to accommodate with the customer demands, controlling the quality of the raw ingredients is crucial in maintaining the quality of the product. For example, orange juice used for popsicle have varying degree of sweetness depending on the time of the year and climate conditions. [2] Controlling the input ingredient's properties will help with achieving desirable product, so the orange juice is needed to be processed before it could be used as feeding material such as concentrating it to the process' standard concentration. In addition to the quality control, transportation cost of moving raw produce to the processing facility cost is quite high due to the energy involved. Reducing the weight and volume of the material will lower this cost by a substantial degree.

2.2 Slurry ice

Slurry ice is the term used to call a mixture of very small ice particles suspended in a solution of water and freezing point depressant. The ice particles range from as small as 1 μm and as big up to 2000 μm [3]. In addition to its small particle size another characteristic is its spherical shape making it able to be use with conventional pumps and distribute evenly on the produce. With these 2 factors, slurry ice provides convenience of use and superb ability to rapidly cool the produce and keep it fresh. Slurry ice is suitable for cold storage during transportation as it helps maintain the produce freshness while minimizing the damage from frost in freeze storage.

Figure 1 Slurry Ice
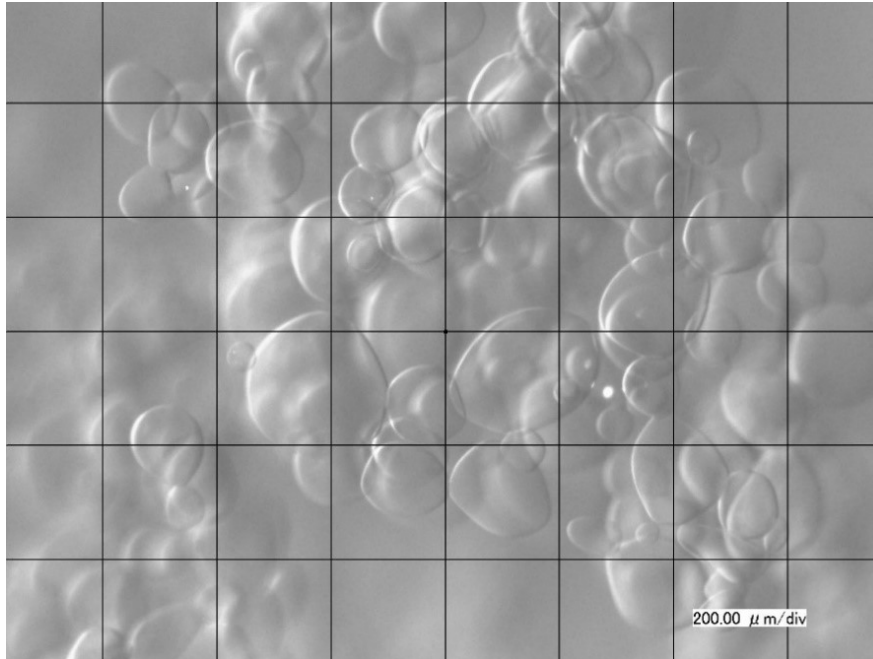
Figure 2 Slurry Ice particle (depressant: salt, 200 μm/div)

2.3 Freezing point depression

A phenomenon where a depressant is added to a solvent to lower its freezing point. These depressants can be regular salt, sugar, alcohol, and many more. This is cause by the decrease in chemical potential of the solution from the addition of said depressants [4]. The degree of freezing point depression is proportional to the molality of the solution, this can be estimated by the following equation below.

$$\Delta T_F = K_F \cdot m \cdot i \tag{2.1}$$

$$\Delta T_F = T_F^0 - T_F \tag{2.2}$$

where ΔT_F : freezing point depression   [K]

T_F^0 : freezing point of pure solvent   [K]

T_F : freezing point of solution   [K]

K_F : cryoscopic constant of solvent   [K kg/mol]

m : molality   [mol/kg]

i : van 't Hoff factor   [-]

Freezing point depression can also be affected from particle size in the slurry. The relationship can be expressed as follow.

$$T_e = T_i^* \left(1 - \frac{2\sigma}{r\rho_I L}\right)$$ (2.3)

where

σ : interfacial tension [J/m²]

T_i^* : solution initial FP [K]

T_e : solution FP at particle radius r [K]

r : particle radius [m]

ρ_I : ice density [kg/m³]

L : latent heat of fusion [J/kg]

2.4 Freeze concentration

The cost of transportation and storage of fruit juice are directly influenced by the weight and its volume. To reduce this cost, the juices are concentrated so that with the same sugar contents its weight and volume is lesser than its original state. There are several methods to increase the concentration by removing the water content from the juice. Conventional thermal evaporation is the most common for liquid food but this leads to the degradation of aromas and other compounds in the juice that are volatile and susceptible to heat degradation. This results in a product that are deemed lower quality than its original state.

Freeze concentration is a process of removing the water contents from the juices in the form of ice crystals. The liquid is cooled to its freezing point where the water contents partially freezes into ice which will then be removed later. The removed ice crystals are considered high purity in water containing little to no sugar or other compounds. With the ice crystals removed, the concentrate results in a higher concentration when compared to its initial state. The concentrate was then cycled back to the process again until the desired concentration is reached.

Freeze concentration have 2 types, suspension where the crystals are separated and grow individually in a stirred tank, and progressive where the ice were generated and grow as a single big block.
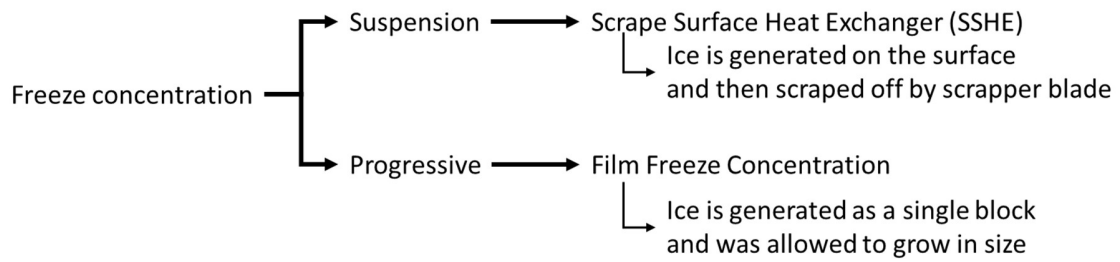
Figure 3 Types of Freeze Concentration
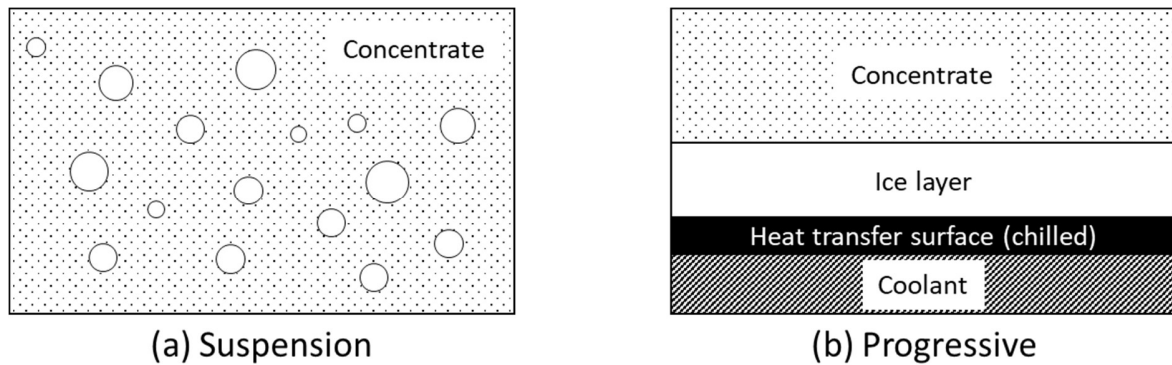
Figure 4 Suspension and progressive Freeze Concentration

The suspension method has 3 major stages: generation, growth, and separation [5]. Each stage has its own equipment dedicated to the job, Scrape Surface Heat Exchanger (SSHE) for ice generation, recrystallizer for ice crystal growth, and centrifuge or wash column for ice removal. The generalized diagram of a scrape surface heat exchanger freeze concentration process is as shown in figure 5.
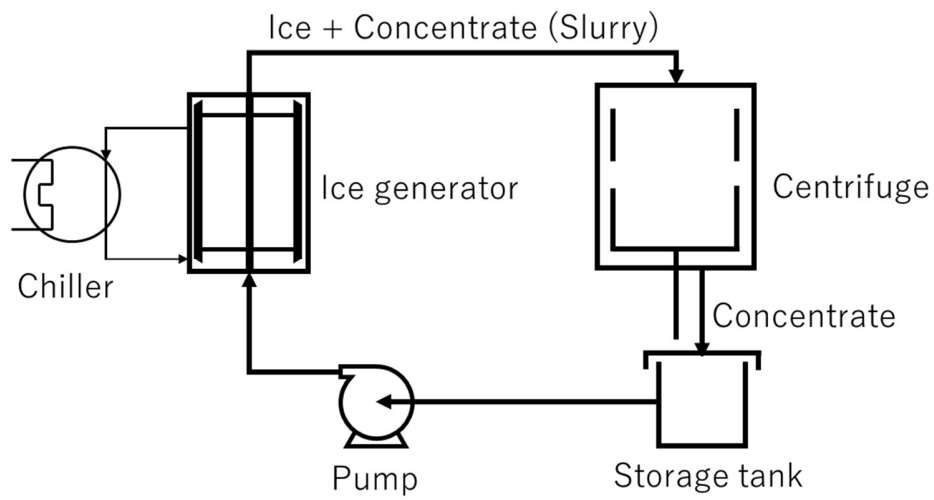
Figure 5 Freeze concentration process flow (SSHE)
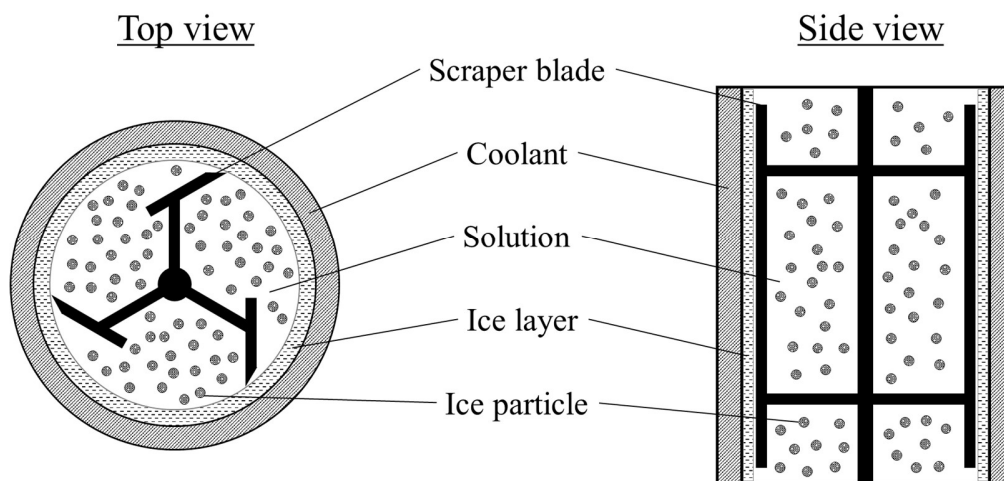
Figure 6 Scrape Surface Heat Exchanger

2.5 Capillary action

Capillary action (also capillary effect) refers to the liquid flow characteristics in narrow spaces without having external forces acting, such as gravity or pressure difference, upon it. This phenomenon can be seen in a thin tube, like straw, where the liquid level in the tube is higher than the bulk of it. It occurs due to the intermolecular forces between the liquid and the surface it adheres to. This phenomenon can also occur in a porous material. In slurry ice, the ice particle is small and packed closely to each other enough to cause this phenomenon to occurs [6].
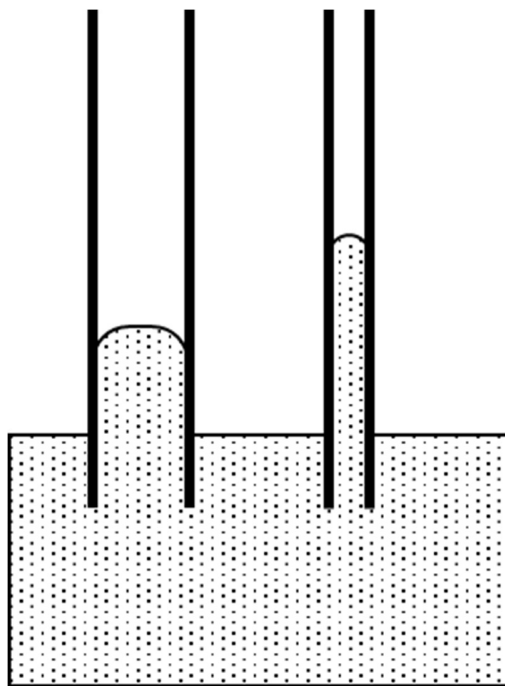
Figure 7 Capillary action in thin tubes
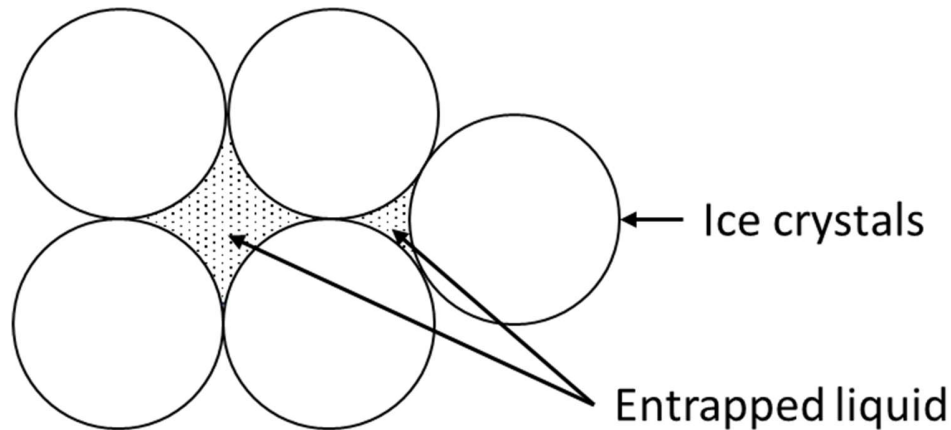
Figure 8 Entrapped liquid

This phenomenon can lead to the liquid loss in the solid-liquid separation step of freeze concentration process. The capillary effect will cause the concentrate to adhere to the surface of the ice particles which is hard to efficiently remove.

2.6 Ostwald Ripening

Ostwald ripening is a phenomenon occurs in a solid-liquid suspension solution where the particle in suspension grows in size due to mass transfer. This phenomenon is thermodynamically driven because larger particles are more stable when compared to smaller counterparts [7]. The atoms at the surface of a particle is energetically unstable when compared to the interior counterparts. This cause large particles to be more favorable because the larger the particle is lesser its surface areas becomes when compared to its volume (specific surface area). With this, the system will try to lower its overall energy by increasing the particles size in expense of smaller particles. Mass transfer occurs within the solution, molecules at the surface of smaller particles detaches and become free molecules which is diffused into the solution. These free molecules then move and condense on the

11

surface of larger particles [7]. This results in large particles increase in size, and smaller particles shrinks or dissolved entirely.
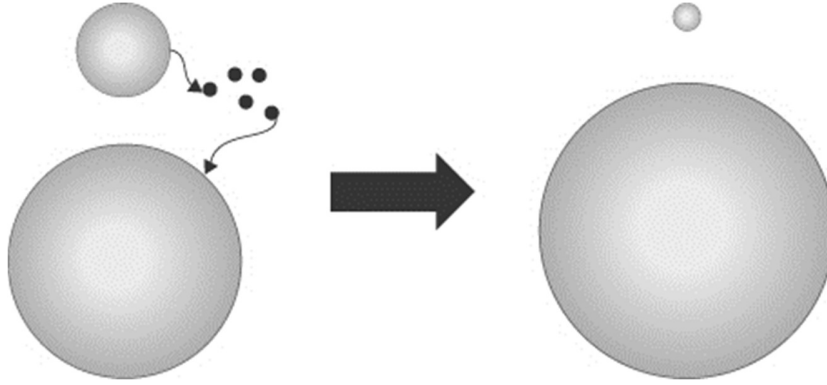
Figure 9 Ostwald ripening (not to scale)
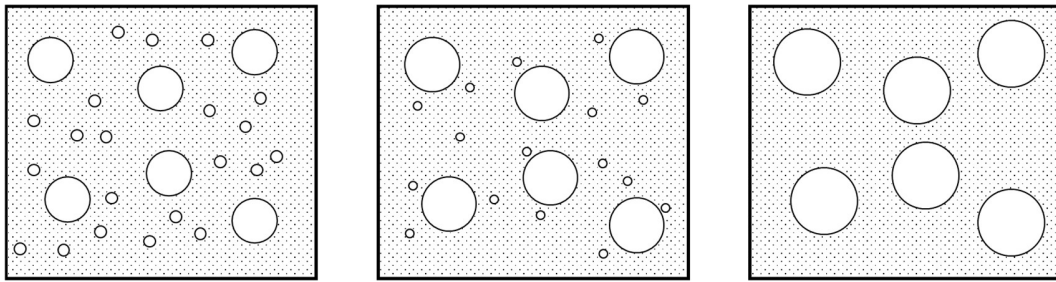
Figure 10 Ostwald ripening (not to scale)

Lifshitz and Slyozov (1961) [8], and Wagner (1961) [9] made the model describing the growth characteristics of ice particle from the effect of Ostwald ripening independently. Which was then consolidated into the LSW theory.

$$R_t^3 - R_0^3 = K_D t \qquad (2.4)$$

where R_t : particle size at time t

R_0 : initial particle size

K_D : diffusive ripening constant

2.7 The Ostwald ripening model

According to the equation 2.4 describing the growth characteristic of particles via Ostwald ripening, a theoretical model was created [10].
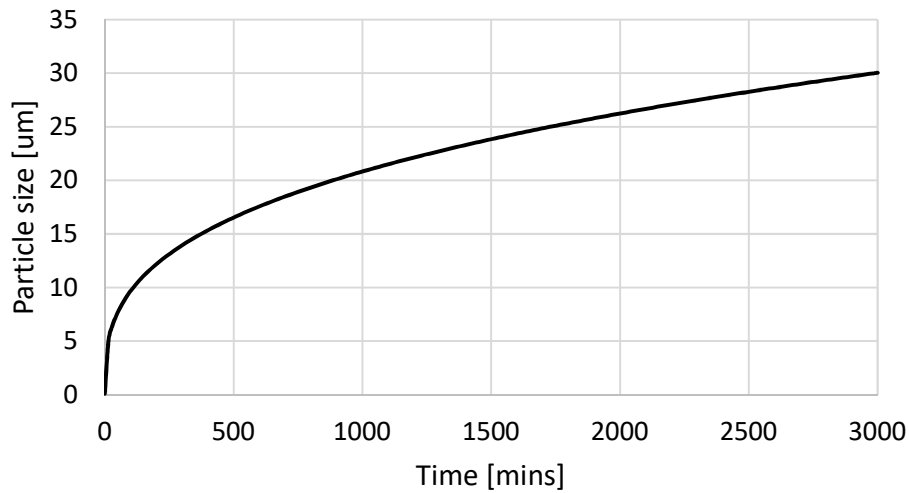
Figure 11 Ostwald ripening model forecast (Theoretical)

The early period of ripening causes the particle to grow rapidly in size. As time passes and the particle became considerably large, the growth starts to change into a linear pattern.
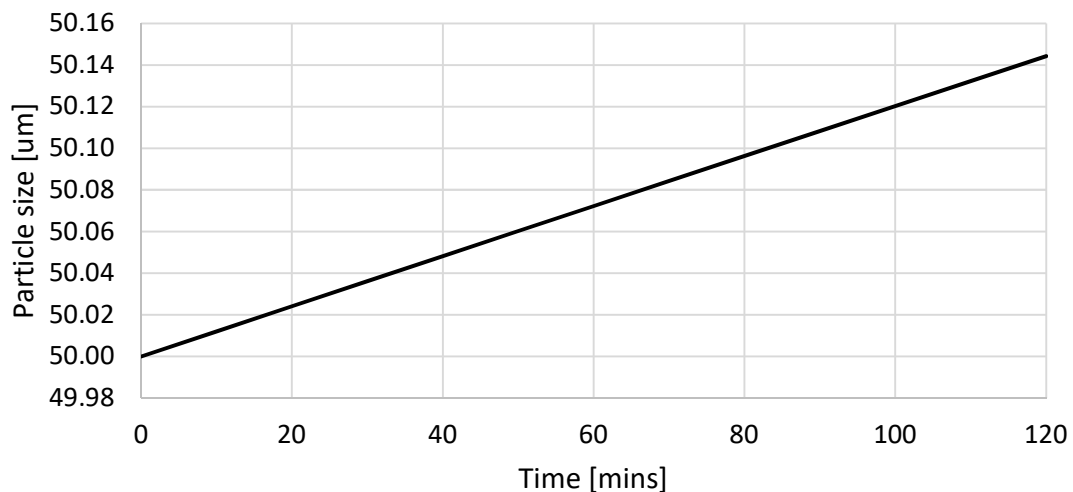
Figure 12 Ostwald forecast from 50 μm onwards

Chapter 3 Ostwald ripening confirmation

Confirmation that Ostwald ripening can occurs to ice particles in slurry ice is necessary and to see the general results that could be expected in the main experiment of this study.

Solution for ice generation was prepared at 1%wt NaCl solution and filled into a thermal insulation sheet lined, 140 liters propylene storage tank (Kaisuimaren Co.Ltd., MH-140). The ice was generated by using the Shakittomini (Izui iron works Co.Ltd., Shakittomini) and transfer to the storage tank. The slurry was kept in suspension by applying agitation at 300 RPM using motorized agitator (HANWAKAKOKI Co.Ltd., KP-4001A). The particle size was measured by using a microscope (KEYENCE, VHX-500F) to photograph the ice particle every 15 minutes starting from when ice starts to appears in the storage tank. Feret diameter [11] was used to measure in this experiment.
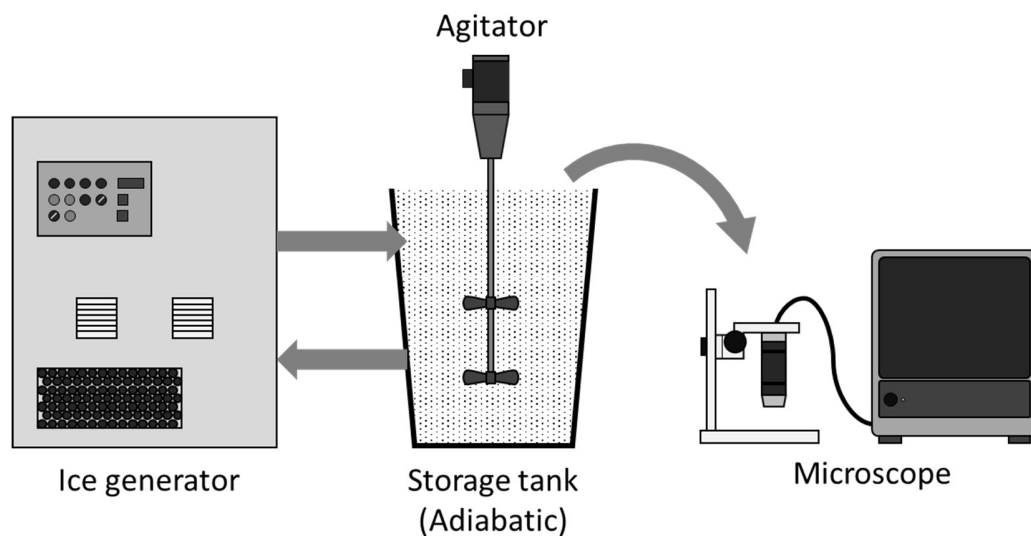
Figure 13 Experiment equipment and set up

3.1 Results

The ice particle size growth rate characteristics can be seen in the figure below. An estimated growth model results at r_t = 16.292 $t^{0.5775}$, with a R-square value of 0.9862 which represents a good correlation of the model. The obtained result corresponds to Ratke and Thieringer findings in 1985 [12] where the time relates to the power 2 of particle size, as shown in the model below.

$$R_t^2 - R_0^2 = Kt \qquad\qquad (3.2)$$

where K : ripening constant
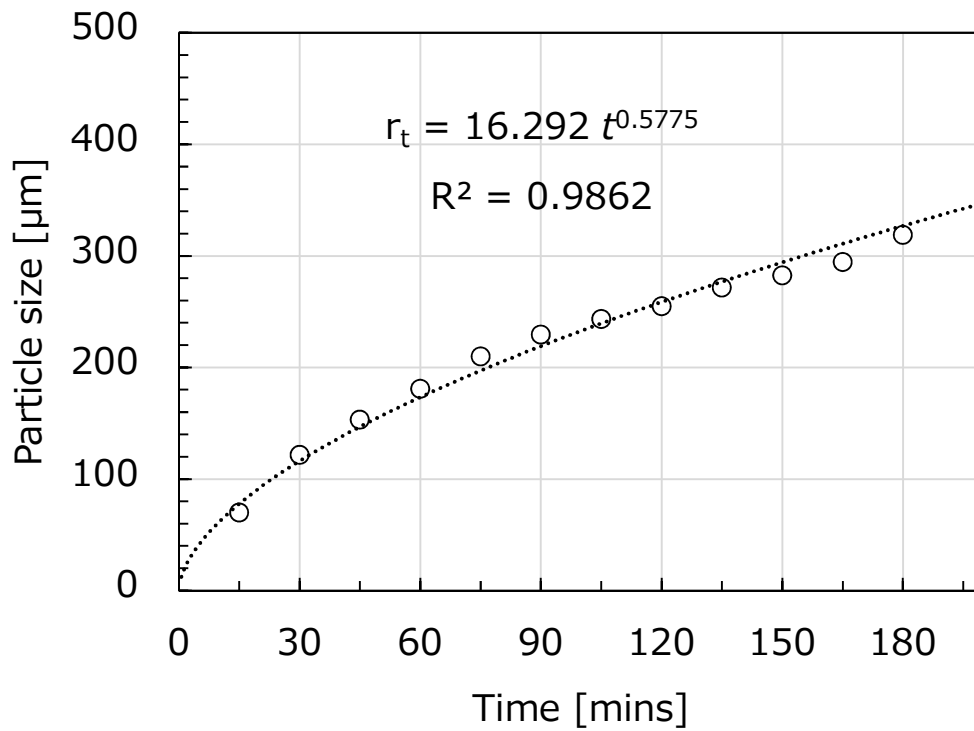
Figure 14 Particle size curve

During the run, very large ice particles very seen from 75 minutes onwards after the initial ice generation. As shown in the following figure below. The super large particle measured to be at around 1mm wide. Considering that this process is adiabatic, no mass was added or removed from the system this crystal growth can be said to be affected by Ostwald ripening.
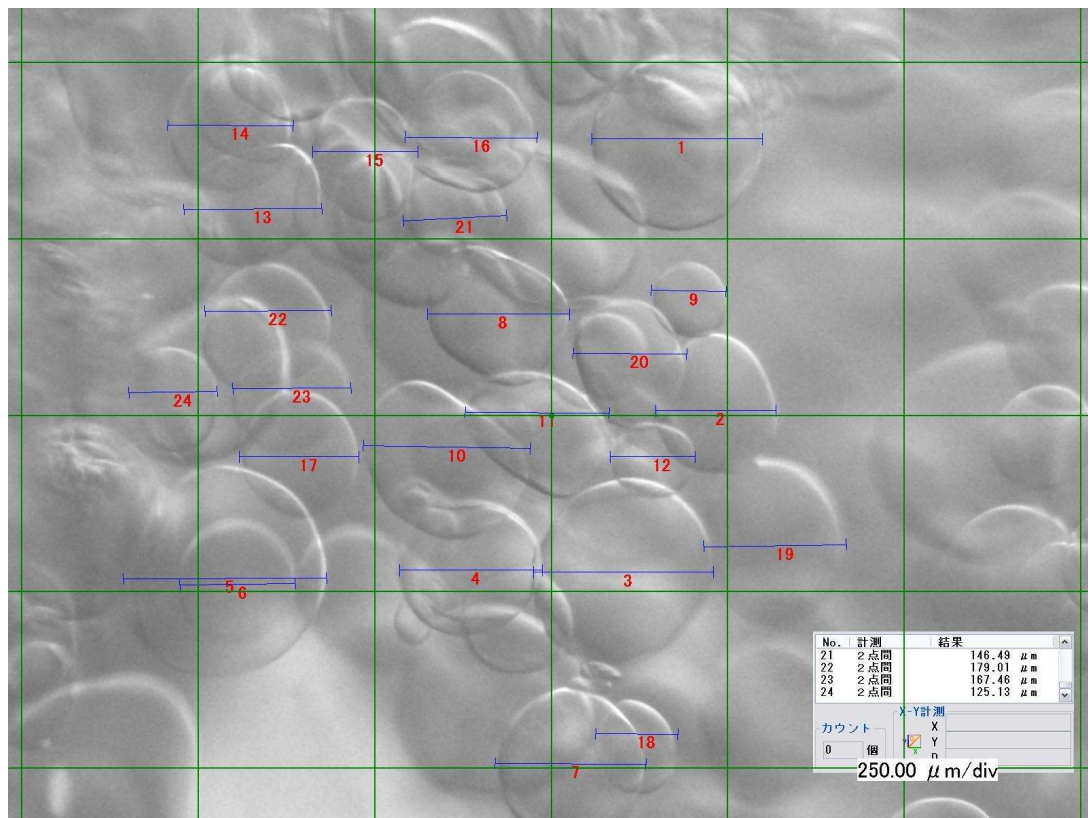
Figure 15 Ice particle (250 µm/div)

(a) 15min　　(b) 30min　　(c) 60min

(d) 120min　　(e) 180min　　(f) 75min
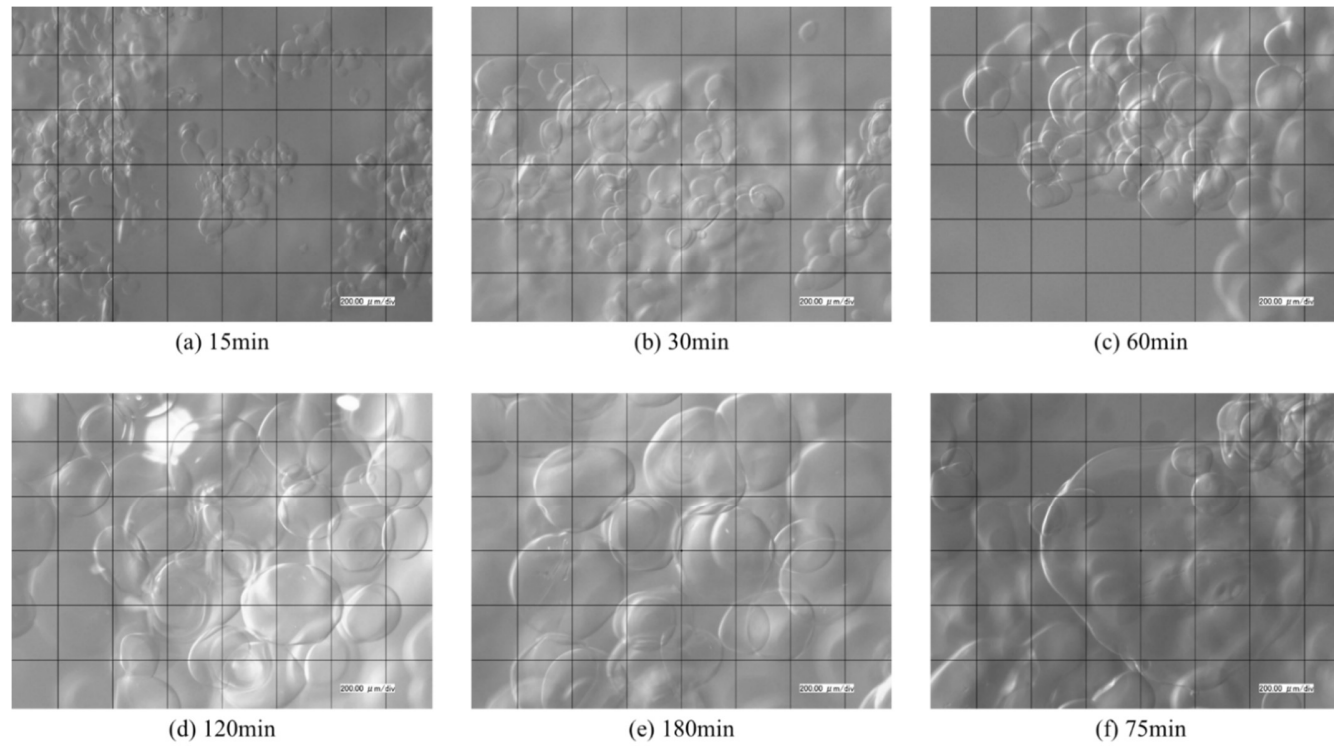
Figure 16 Ice particle (microscopy, 15 minutes intervals)

Table 1 Particle size and deviation

Time	15	30	45	60	75	90	105	120	135	150	165	180
Average	69.99	121.80	153.25	180.86	209.87	229.61	243.57	254.82	271.61	282.67	294.58	318.91
Median	65.47	118.38	153.05	179.97	204.07	230.99	243.50	248.30	275.74	287.84	299.32	324.65
Deviation	6.46	2.81	0.13	0.49	2.77	-0.60	0.03	2.56	-1.52	-1.83	-1.61	-1.80

Chapter 4 Experiment design, methodology, and analysis methods

This chapter will discuss about the main experimental equipment design and method of this study.

4.1 The equipment

In suspension freeze concentration each module has its own dedicated job. The generator module, a scraped surface heat exchanger (SSHE), produces ice crystal by cooling the feed liquid using cooling jacket and scrape off the ice formed at the cooling surface by a rotating scrapper blade. The recrystallizer facilitates ice crystal growth by providing suitable ripening temperature and homogeneous mixing. These two modules have its own optimum operating conditions so it cannot be combined into one single module.

The ice particles were generated by a scraped surface heat exchanger (SSHE) then fed into the recrystallizer module and looped back. The main body and the cooling jacket were made with stainless steel. The outer surface of the cooling jacket was lined with thermal insulation to prevent unwanted heat transfer with the surroundings. To increase the efficiency of the cooling process the upper and lower portion were made with polypropylene that has low heat transfer rate and the piping were also lined with thermal insulating material.

The solution was fed into the entry point at the bottom of the generator and exits at the top, this ensures that the solution takes the whole space in the generator and maximizes the cooling capability of the equipment. The coolant also flows in the same manner, fed in from the bottom and exits at the upper valve. The entry point and exit point were off-set to the side to provides a good circular flow of the coolant in the jacket. Oil-seal were installed to the rotating scrapper-blade shaft to make a liquid tight seal while also letting the shaft rotate freely.
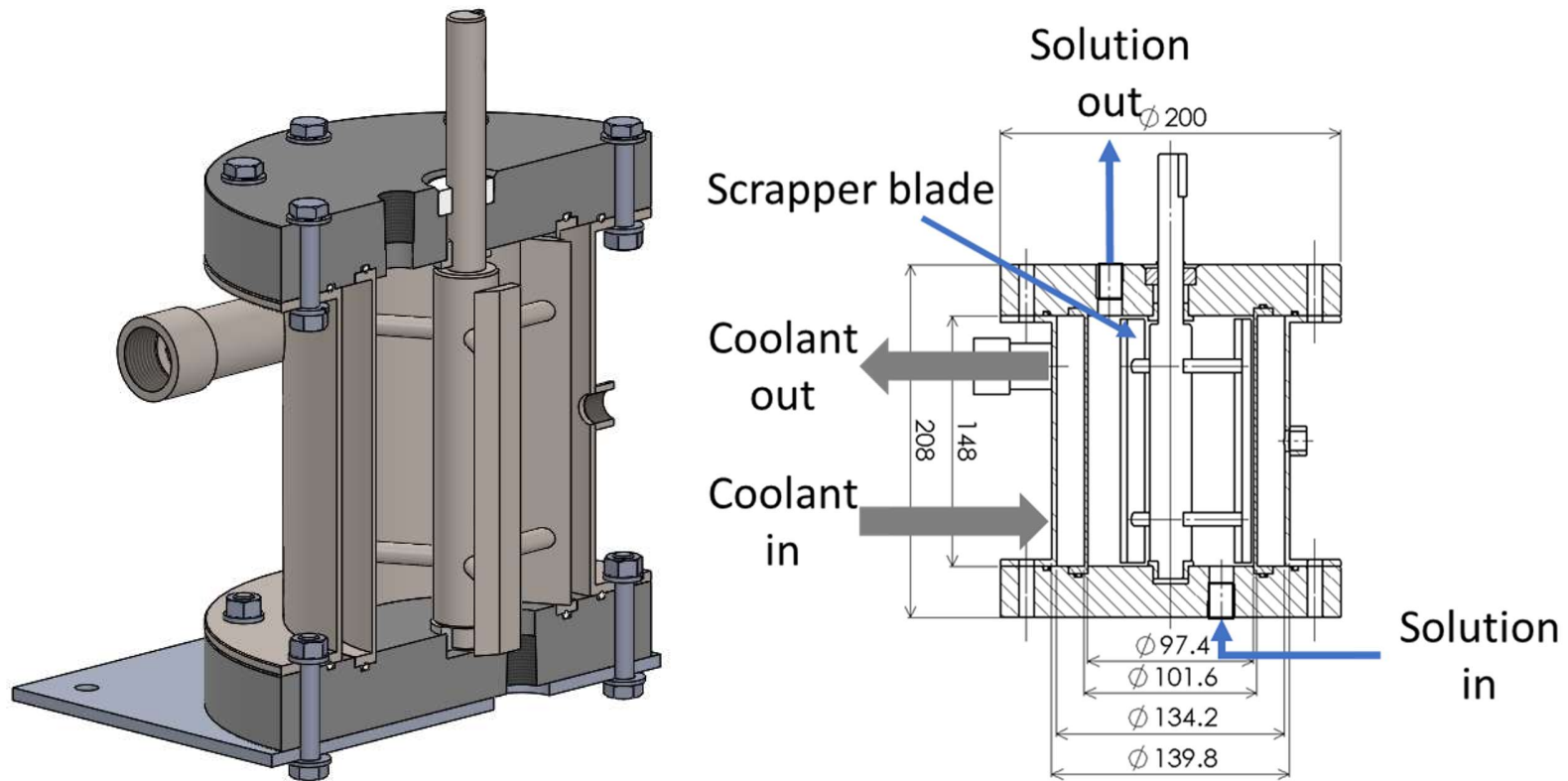
Figure 17 Ice generator

The recrystallizer provides agitation the bulk liquid to prevent particle from agglomerating together, and provides suitable temperature for the particles to grow (ripen). A simple design was made with these 2 specific properties to fulfill. Stainless steel was used to produce the main body. The cover was made out of transparent acrylic to be able to see the inner parts of the module. The 2 parts are then clamped together by 8 bolts with rubber O-ring in-between the seams to make a liquid tight seal. The inside of the recrystallizer was installed with 4 baffles to help achieve homogenous mixing in the module. The agitator shaft cavity was sealed with an oil-seal and other connective threads was wrapped with Teflon tape before tighten to the module.
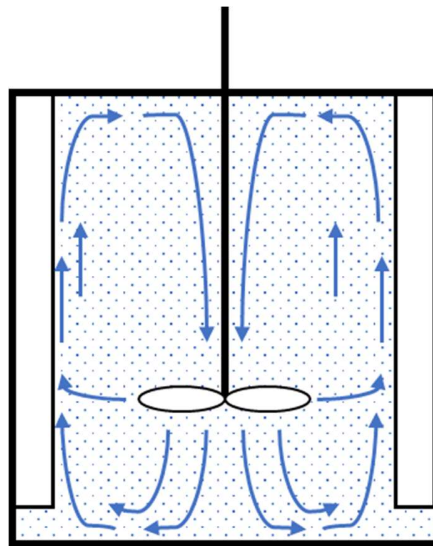
Figure 18 Flow pattern in a baffled stirred tank
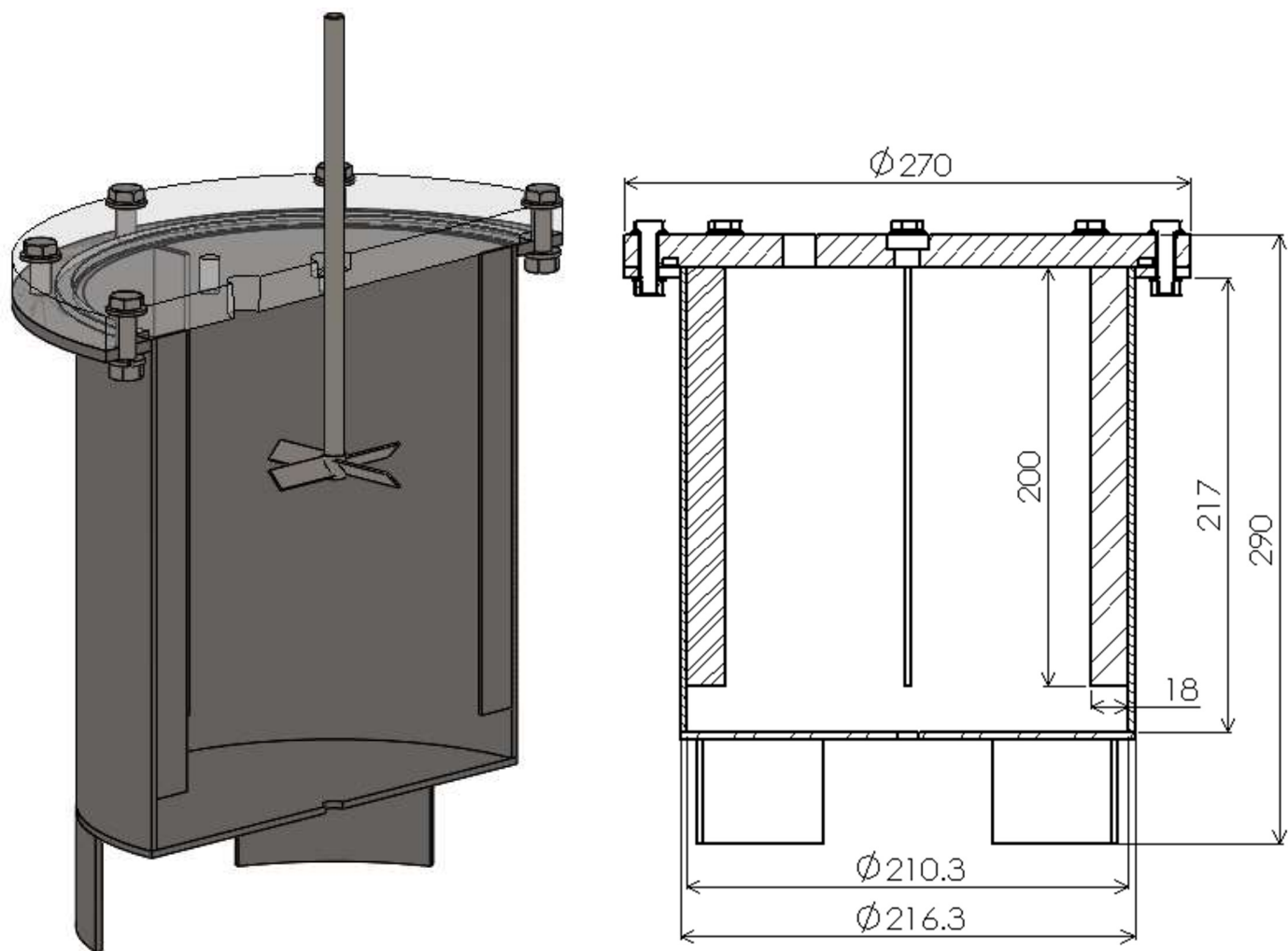
Figure 19 Recrystallizer

The motor (IKA, EUROSTAR20-digital) with a range of 30 − 2000 RPM was used to rotate the agitator. A torque meter (Unipulse, UTM II-10Nm) was installed between the motor and the agitator rod. A magnetic pump (SANSO Electric Co.Ltd., PMD-331B6C) was used to pump the liquid within the system.

The system has a total liquid capacity of about 9 liters this include the liquid in the pipe lines and pump, with the recrystallizer occupying about 7.7 liters. 60%wt ethylene glycol was used as a coolant for the generator module.
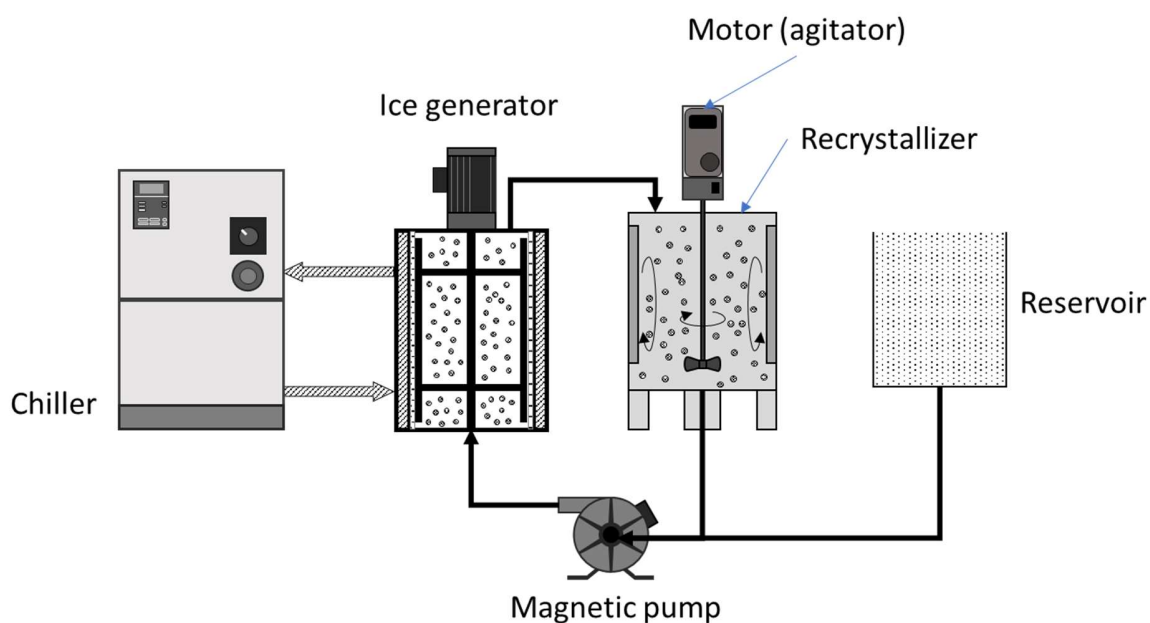
Figure 20 Overall experiment schematic

4.2 Methodology and conditions

The operating room was kept at the lowest, stable temperature of 15°C. Other equipment that produces large quantity of heat were placed outside of the room, such as air compressor, and chiller.

The SSHE coolant was kept at -12°C during the first 30 minutes of ice generation and increased to -2.7°C during cold storage. This was done to counteract the unavoidable heat produced from the pumps and agitation. And also, to simulate a system where the ice particles were continuously removed from the loop resulting in a near constant ice packing factor (IPF). At -2.7°C the amount of ice production balances out with the amount of ice melted from the heat. If the ice generator were to produce ice for the entire iteration the amount of produced ice will be large enough to reduce the solution flow to near 0 L/min or totally block the flow.

The recrystallizer agitation speed used in the experiment was calculated from rotational Reynolds number ranging from Re_r 10,000 to Re_r 45,000.

$$Re_r = \frac{\rho D N}{\mu} \qquad (4.1)$$

where Re_r : rotational Reynolds number   [-]

ρ : solution density   [kg/m^3]

D : agitator's diameter   [m]

N : rotation speed (RPM)   [min^{-1}]

μ : solution viscosity   [Pa·s]

Table 2 Experimental conditions

Ice Generator				Recrystallizer		
Concentration	[°Brix]	10				10,000
Volume	[L]	8				15,000
Scrapper speed	[min^{-1}]	360				20,000
Rotational Reynolds ()	[-]	22453		Rotational Reynolds (Re_r)	[-]	25,000
Solution flow rate	[L/min]	10 → 5				30,000
Coolant temp.	[°C]	−12 → −2.7				35,000
Coolant flow rate	[L/min]	35				40,000
						45,000
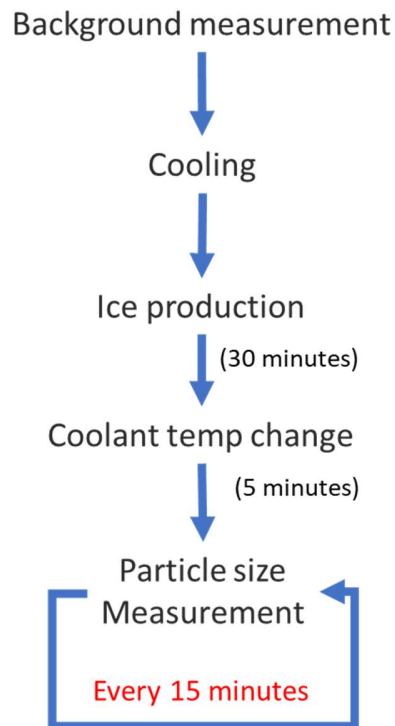
Figure 21 Experiment procedure

While the experiment is running, after 30 minutes of ice production the coolant temperature was increased from -12°C to -2.7°C and held for 5 minutes until the temperature reaches the new equilibrium. After it reaches the new temperature, the pump power was reduced to have a liquid flow rate of 5 liter per minute (measured be the entry point of ice generator). This marks as the 0-minute mark for the run. From this point onwards, every 15 minutes particle size was measured and solution sample was taken to monitor the change in concentration which in turn will represent the ice packing factor of the slurry in the system.
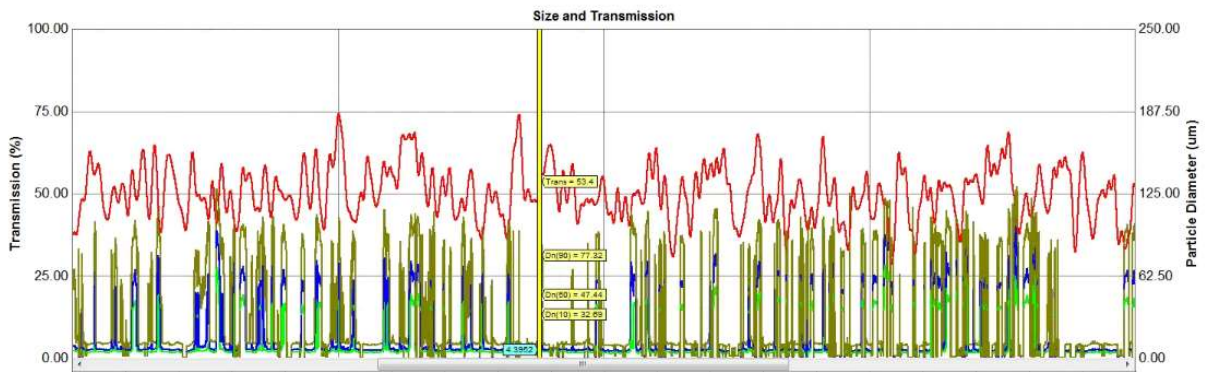
Figure 22 Normal measurement results
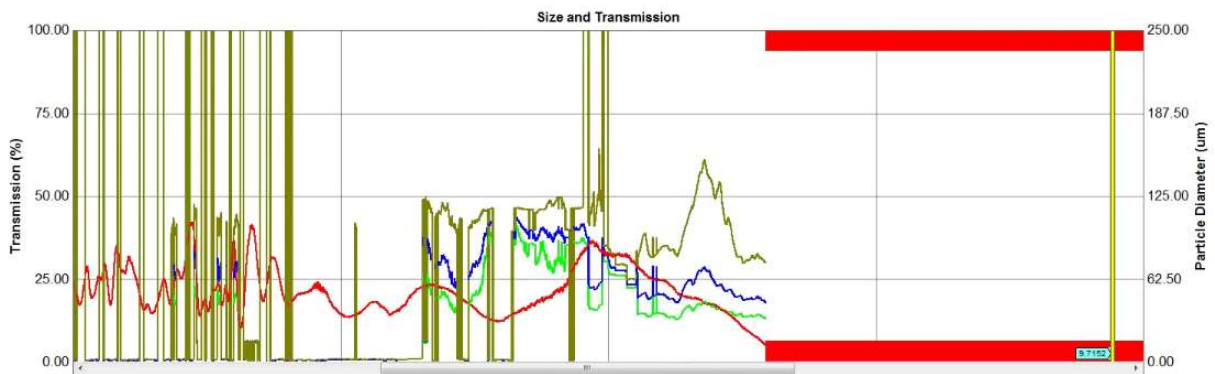
Figure 23 Not enough particle results

If particle size measurement were to be done at the moment ice was generated, the amount of ice particle will not be enough to be measured. As can be seen in the figures above. A normal result will have a considerable amount of data to use, while a result where the particle is not enough will produce little to no usable data. The red area indicates the portion where the equipment could not collect data, either the laser beam was entirely blocked or there was no particle for the laser to diffract.

27

4.3 Ice packing factor

Ice packing factor (IPF) represents the mass fraction of ice to the total mass of the solution [13]. IPF is defined as:

$$IPF = \frac{m_{ice}}{m} \qquad (4.2)$$

where m_{ice} : ice mass   [kg]

m : total mass   [kg]
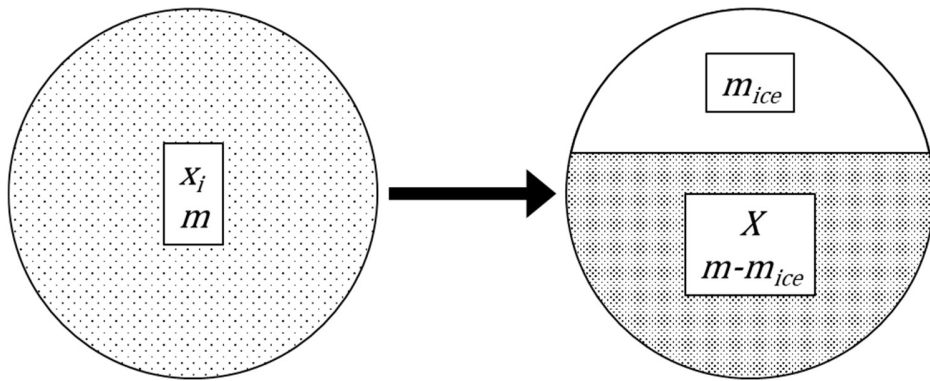
Figure 24 Slurry ice IPF

In the initial state where ice is not present the x_i is the initial concentration by weight of the solution.

$$x_i = \frac{m_{solute}}{m} \qquad (4.3)$$

After ice is generated the concentration of the solution in the system increases. This happens because a single ice crystal is considered pure water (theoretically).

$$x = \frac{m_{solute}}{m - m_{ice}} \qquad (4.4)$$

With the 2 equation above, rearrange and *IPF* can be defined as a correlation to solution's concentration as:

$$IPF = 1 - \frac{x_i}{x} \qquad (4.4)$$

where x_i : initial concentration   [%wt]

          x : concentration   [%wt]

       m_{solute} : solute mass   [kg]

4.4 Particle size measurement

Particle size were measured using laser diffraction equipment (Malvern, Spraytec). The particle feeds into a wet cell measurement apparatus where it will come in contact with the laser and diffract it, which will later be picked up and calculate the particle size from the data.
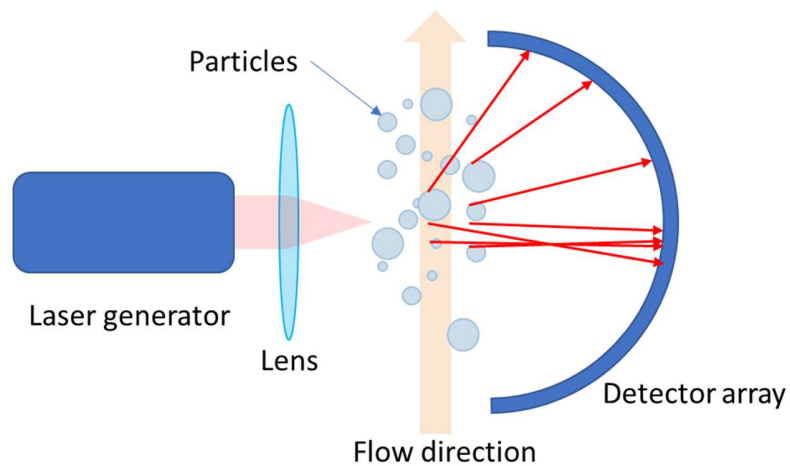
Figure 25 Laser diffraction

Figure 26 Spraytec (Malvern)

The measurement results were displayed as a particle size distribution curve. The parameter used to represent and compare the results are D_{10}, D_{50}, D_{90}, and sauter mean diameter. Dn represents the particle size where it corresponds to $n\%$ cumulative number. In general, D10 represents particle size at the 10th percentile, 10% of all measured particle is lower or equal to the particle size. [14]
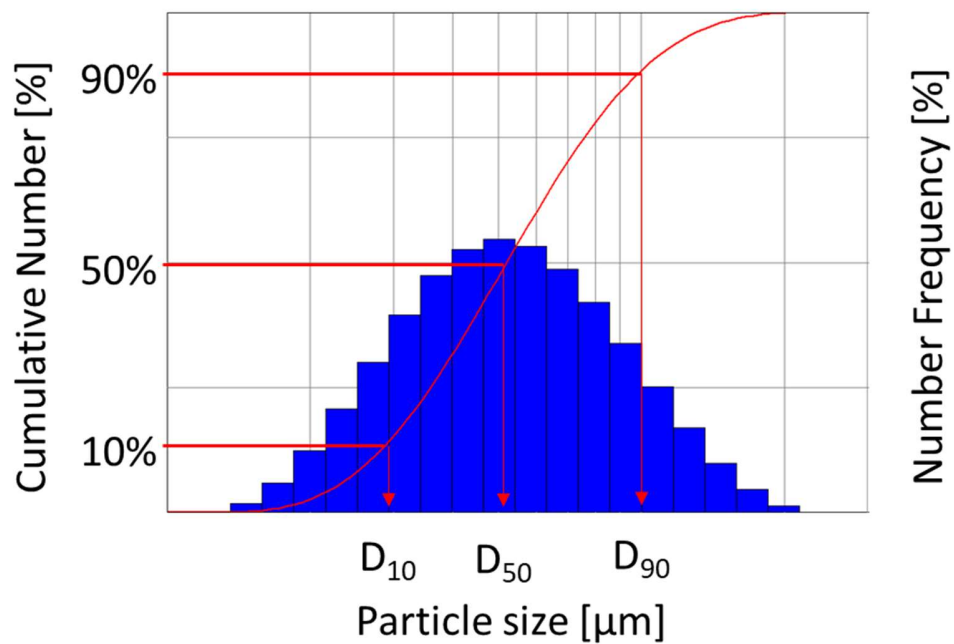
Figure 27 Particle size distribution curve

4.4.1 Sauter mean diameter (SMD)

Sauter mean diameter is a representation of the average particle size developed by Josef Sauter [15]. SMD was defined as the diameter of a sphere that has the same volume to surface area ratio as a particle of interest. [16]

$$d_{32} = \frac{d_V^3}{d_S^2} \tag{4.2}$$

$$d_V = \left(\frac{6V_p}{\pi}\right)^{1/3} \tag{4.3}$$

$$d_S = \sqrt{\frac{A_p}{\pi}} \tag{4.4}$$

where d_{32} : sauter mean diameter

d_V : volume diameter   [m]

d_S : surface diameter   [m]

V_P : particle volume   [m³]

A_P : particle surface area   [m²]

4.5 Results and discussion

In this section the results of the experiment will be discussed. The following part will be divided into 3 main sections. The low, medium, and high agitation range.

The range were determined by the agitation characteristics during the run. Low meaning that the power was not enough to achieve homogeneous mixing to the solution in the recrystallizer. Medium range is where homogeneous mixing was achieved and the surface of the solution was relatively stable with no vortex forming. Finally, high range is where the agitation power was very high and creates a small vortex at the surface of the solution but not enough to introduce air bubbles into the solution causing frothing.

As stated earlier in chapter 2, Ostwald ripening in particle size with large initial size can be considered as a linear model, the following discussion will be using this concept to describe the relationship of particle size and time, particle growth.

For each condition, the samples were measured for their respective concentrations and the IPF value were calculated as stated earlier in this chapter. Most of the conditions produces a fairly constant IPF from the 35 minutes mark onwards. This represent that the amount of melted ice matches the amount of newly produced ice.
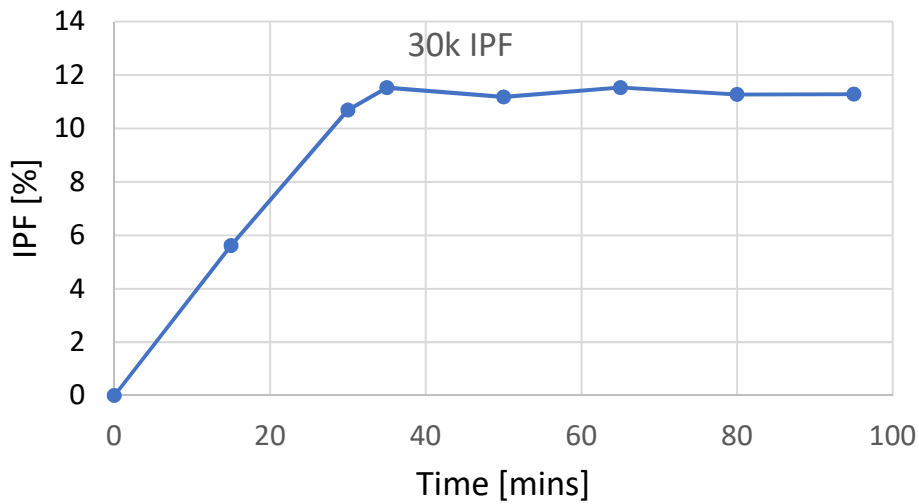
Figure 28 Re_r 30,000 IPF

4.5.1 Low (Re_r 10,000 − 20,000)

During the run, ice particles starts to accumulate at the upper portion of the recrystallizer module. This cause a non-homogeneous mixing within the recrystallizer hindering the particle growth significantly. What agitation provides is the remove the mass transfer limit due to diffusion speed of solute in the bulk liquid. If ice can accumulate at the top portion this means the power wasn't enough. Re_r 10,000 have the thickest ice layer and this thickness decreases as the Re_r increases. At Re_r 20,000, ice layer was still present but it didn't persist for the entire run, it periodically forms and disintegrate for the whole iteration. All results can be seen in the appendix.
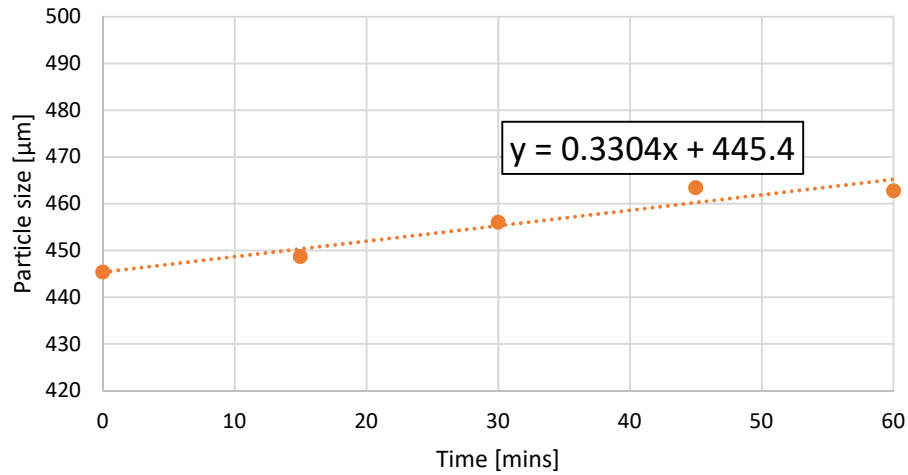
Figure 29 Re_r 10,000 sauter mean diameter
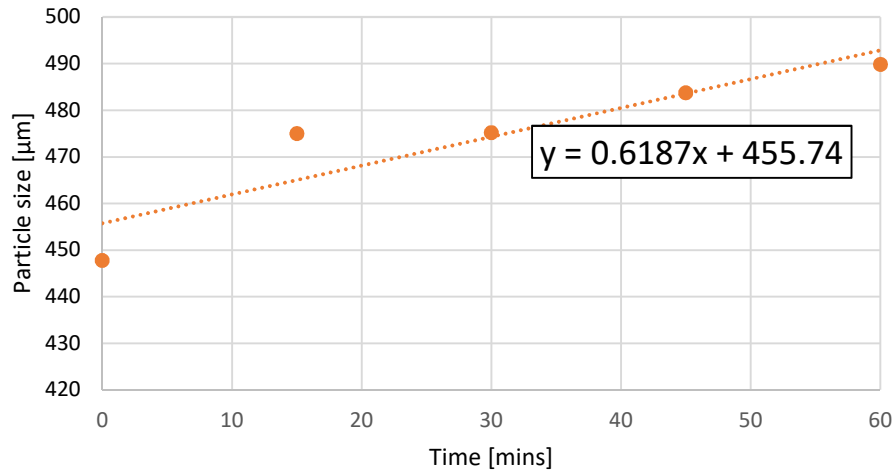
Figure 30 Re_r 20,000 sauter mean diameter

The growth rate of each Re_r, when compared to each other, have an increasing trend. In which Re_r 10,000 has the lowest (0.33 µm/min) and Re_r has the highest growth rate (0.62 µm/min) in the grouping. This happens from the degree of agitation provided by the agitator. The main controlling factor of particle growth by Ostwald ripening is the mass diffusion rate in the bulk solution [3]. Higher agitation assisted in accelerating the mass diffusion, in turn makes the ice particle grow quicker.

In addition, the initial particle size was different in all runs within the range, Re_r 10,000 have the lowest initial particle size while Re_r 20,000 have the largest in the range. This is something that could be researched further in the future. This was the effect of agitation in the first 30 minutes of ice production, which particle size was not measured due to limitations of the particle size measuring equipment as discussed earlier in this chapter.

4.5.2 Medium (Re_r 25,000 – 30,000)

In the medium range, a significant increase in ice particle growth can be seen. Albeit having a smaller initial particle size, a growth rate of 0.82 μm/min was a significant jump from 0.33 μm/min of Re_r 10,000.
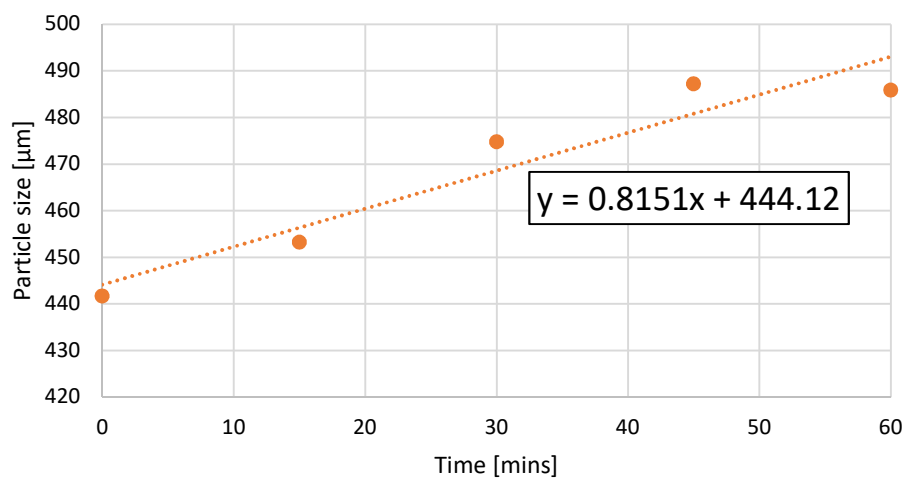

y = 0.8151x + 444.12

Figure 31 Re_r 30,000 sauter mean diameter

During the experiment a promising sign was noticed, the ice layer that usually forms at the upper portion of the bulk liquid disappear entirely. As oppose to the low range where the layer forms and disintegrate periodically, the medium

range agitation is enough to achieve homogeneous mixing in the solution preventing the formation of said ice layer.

4.5.3 High (Re_r 35,000 and above)

High agitation range at Re_r 35,000 was done and the particle grows in the same manner as the previous 2 ranges. The expectation is that the growth rate should be higher when compared to the medium and low agitation range but what happens is in fact lower than the medium range. The Re_r 35,000 has a higher growth rate than the low range but as the Re_r increases the growth rate decrease. As can be seen in the figures below.
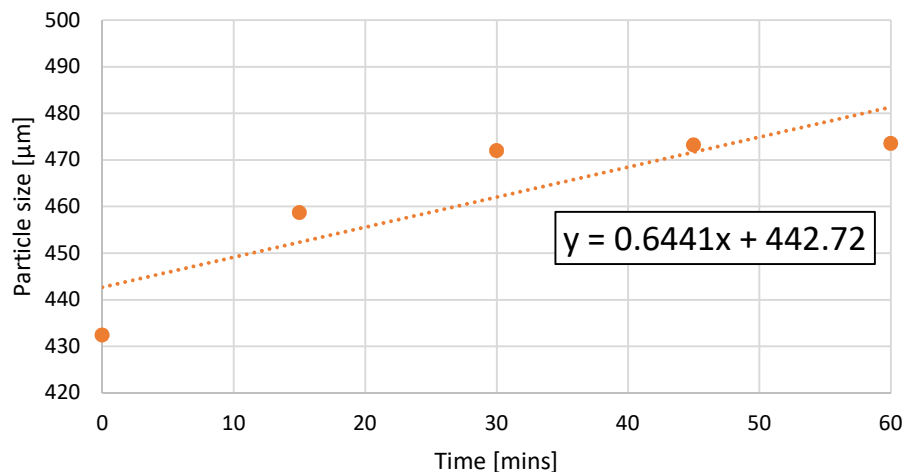

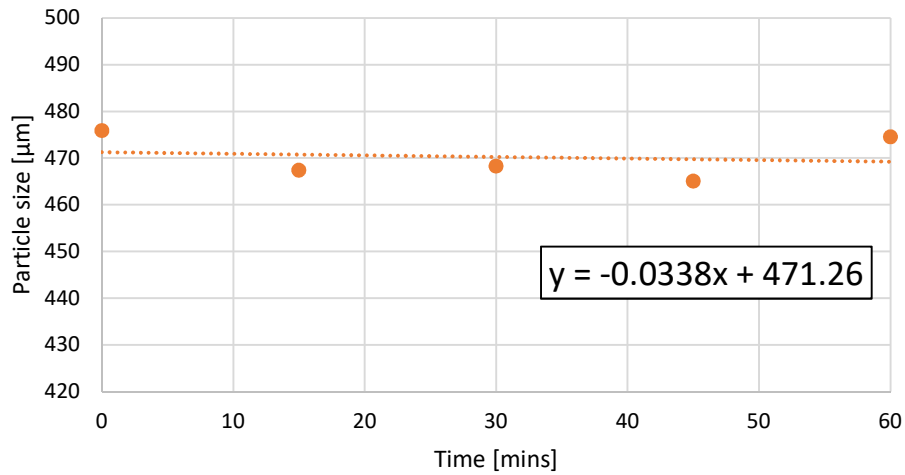Figure 32 Re_r 35,000 sauter mean diameter

Figure 33 Re_r 45,000 sauter mean diameter

This was caused by the heat generated from agitation making the ice melts and the high shear force acting as an inhibitor to the ice particle growth via Ostwald ripening. Even though Ostwald ripening's limiting factor is the mass diffusion rate within the bulk liquid, applying too much will decreases the growth rate. During the Re_r 45,000 run, visible bubbles within the solution cannot be seen but during the data collection from the particle size measurement equipment (Spraytec, Malvern) a lot of noise was found in the results. This was caused by the microbubbles that couldn't be seen by the naked eye but will diffract the laser causing the noise.
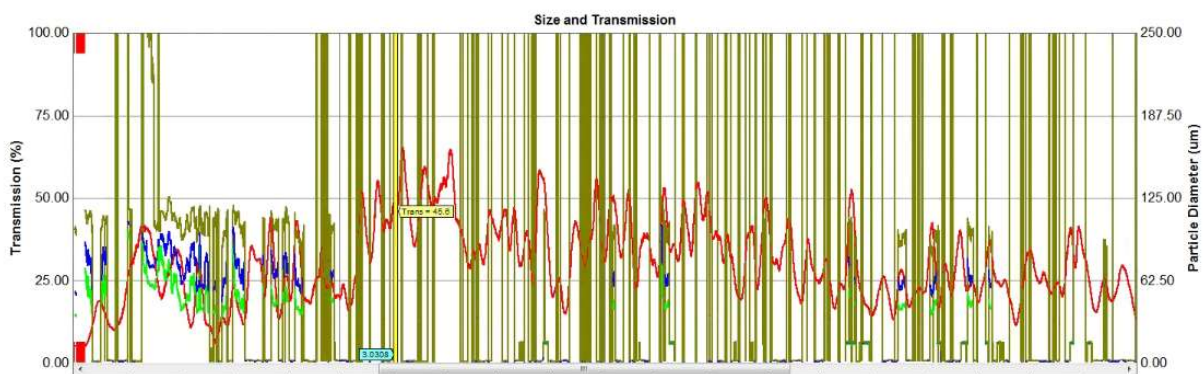

Figure 34 Noise effect from microbubbles

4.5.4 Growth rate and Re_r relationship

Considering each individual condition leads to the question of what relationship between the growth rate and the Re_r have to each other. With all the available data, a consolidated curve can be formed.

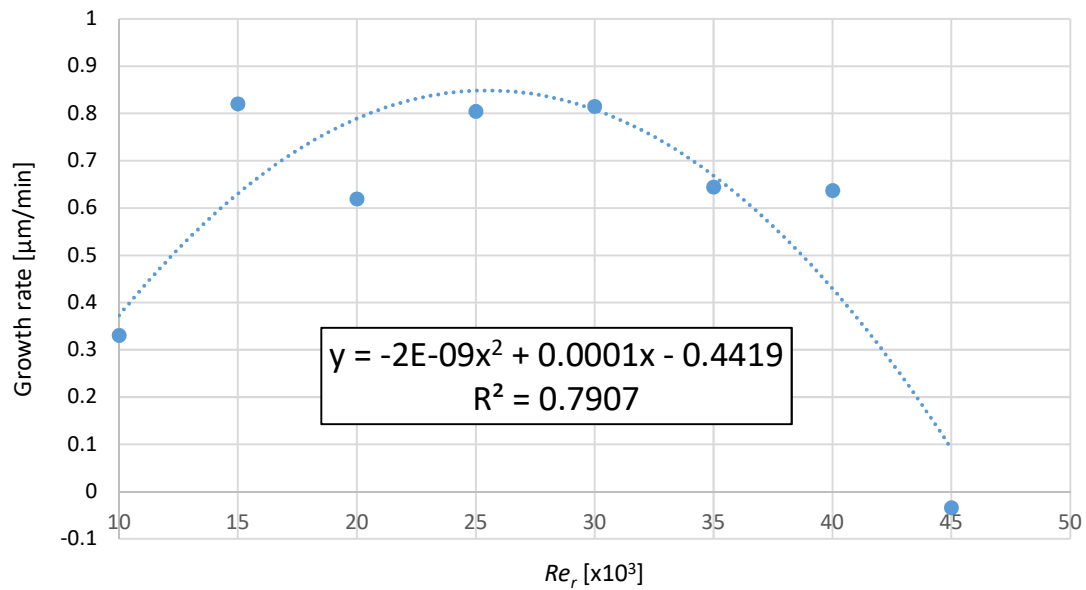$$y = -2E\text{-}09x^2 + 0.0001x - 0.4419$$
$$R^2 = 0.7907$$

Figure 35 Sauter Growth rate and Re_r relationship

A second-degree polynomial can be seen through curve fitting. At first, the relationship function was thought to be a linear relationship but after curve fitting second-degree polynomial model better describes the growth characteristics than the linear model.

Conclusion

Agitation in the cold storage tank of continuous freeze concentration process have a direct effect on the ice particle size. Using low agitation, the ice particles grows at a slow rate, but applying too much agitation will cause the ice to melt. The suitable agitation power for maximum ice particle growth is where it is enough to achieve homogeneous mixing.

Acknowledgement

References

[1] A. Omran and C. King, "Kinetics of Ice Crystallization in Sugar Solutions and Fruit Juices," *AlChe,* vol. 20, no. 4, pp. 795-803, 1974.

[2] H. E. Pattee, in *Evaluation of Quality of Fruits and Vegetables*, New York, The AVI publishing company, inc., 1985, p. 93.

[3] P. Pronk, C. I. Ferreira and G. Witkamp, "A dynamic model of Ostwald ripening in ice suspensions," *Journal of Crystal Growth,* no. 275, pp. e1355-e1361, 2005.

[4] J. Jayawardena, M. Vanniarachchi and M. Wansapala, "Freezing point depression of different Sucrose solutions and coconut water," *International Journal of Food Science and Nutrition,* vol. 2, no. 3, pp. 68-71, 2017.

[5] J. Sanchez, Y. Ruiz, J. Auleda, E. Hernandez and a. M. Raventos, "Review. Freeze Concentration in the Fruit Juices Industry," *Food Science and Technology International,* vol. 15, pp. 303-315, 2009.

[6] "Capillary Action – Liquid, Water, Force, and Surface – JRank Articles," science.jrank.org, 27 5 2013. [Online]. Available: https://web.archive.org/web/20130527124752/http://science.jrank.org/pages/1182/Capillary-Action.html. [Accessed 10 7 2020].

[7] L. Ratke and P. W. Voorhes, in *Growth and Coarsening: Ostwald Ripening in Material Processing*, Springer, 2002, pp. 117-118.

[8] I. Lifshitz and V. Slyozov, "THE KINETICS OF PRECIPITATION FROM," *Journal of Physics and Chemistry of Solids,* vol. 19, pp. 35-50, 1961.

[9] C. Wagner, "Theory of the aging of precipitates by dissolution-reprecipitation (Ostwald ripening)," *Zeitschrift für Elektrochemie,* vol. 65, pp. 581-591, 1961.

[10] S. Abbott, Solubility Science: Principles and Practice, 2015.

[11] H. G. Merkus, "Particle Size Measurements: Fundamentals, Practice, Quality," 2009, p. 15.

[12] L. Ratke and W. Thieringer, "The Influence of Particle Motion on Ostwald ripening in liquids," *Acta Metallurgica,* vol. 33, no. 10, pp. 1793-1802, 1985.

[13] J. H. PECK, C. KANG and H. HONG, "MEASUREMENT OF ICE PACKING FACTOR OF AQUEOUS SOLUTION WITH ICE SLURRY USING REFRACTIVE INDEX," *International Journal of Air-Conditioning and Refrigeration,* vol. 18, no. 2, pp. 149-155, 2010.

[14] H. Y. Saw, C. E. Davies and A. H. Paterson, "The Influence of Particle Size Distribution and," *Chemeca ,* 2013.

[15] S. Josef, Die Grössenbestimmung der in Gemischnebeln von Verbrennungskraftmaschinen vorhandenen Brennstoffteilchen, VDI-Verl, 1926.

[16] F. Scala, "Particle characterization and behavior relevant to fluidized bed combustion and gasification systems," in *Fluidized Bed Technologies for Near-Zero Emission Combustion and Gasification*, Woodhead, 2013, pp. 42-76.

Appendix: Supplement data

Re$_r$ 10,000 data

Table 3 *Re$_r$* 10,000 Particle size data

	0	1	14	16	29	31	44	46	59	61
D10	40.012	40.863	39.679	40.911	42.864	44.615	45.888	45.328	44.168	46.406
D50	54.677	55.391	58.502	57.091	66.598	67.129	67.657	66.112	67.884	67.53
D90	85.367	87.552	94.39	91.615	103.44	104.32	105.15	104.15	103.81	104.78
D43	585.42	583.32	593.45	585.05	605.4	606.89	607.25	594.32	607.98	606.35
D32	443.93	446.91	449.27	448.22	447.44	464.77	469.84	457.12	456.44	469.23

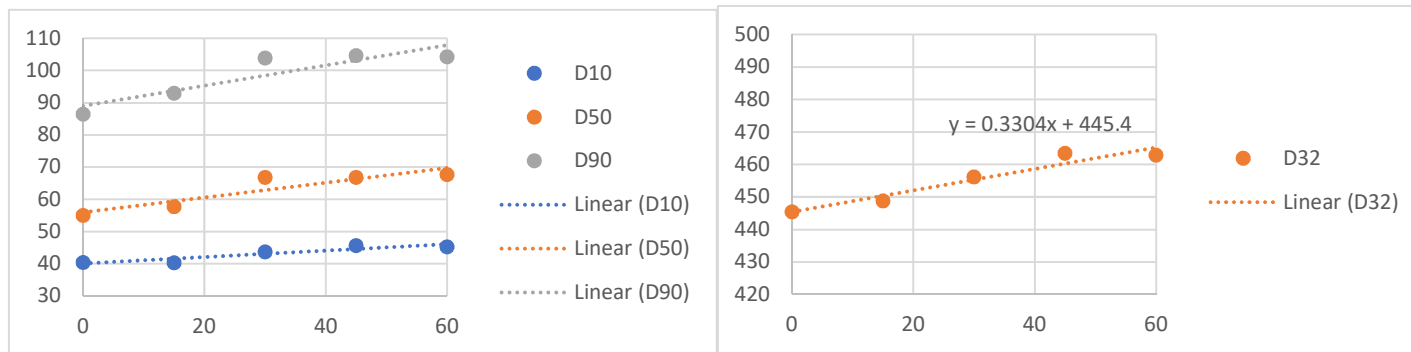Figure 36 *Re$_r$* 10,000 Particle size graphs (D10, D50, D90, SMD)

Re_r 15,000 data

Table 4 Re_r 15,000 Particle size data

	0	1	14	16	29	31	44	46	59	61
D10	38.929	41.277	40.552	41.555	39.812	42.893	42.137	42.562	39.651	32.15
D50	58.05	58.948	57.735	59.535	59.683	60.159	59.651	59.088	58.724	54.102
D90	96.701	94.815	92.386	95.517	96.541	95.248	94.166	94.473	94.376	83.62
D43	554.84	583.34	584.79	590.52	585.19	592.31	591.95	593.34	580.53	427.94
D32	401.26	441.87	442.37	452.64	435.94	458.18	455.57	461.14	431.48	507.44
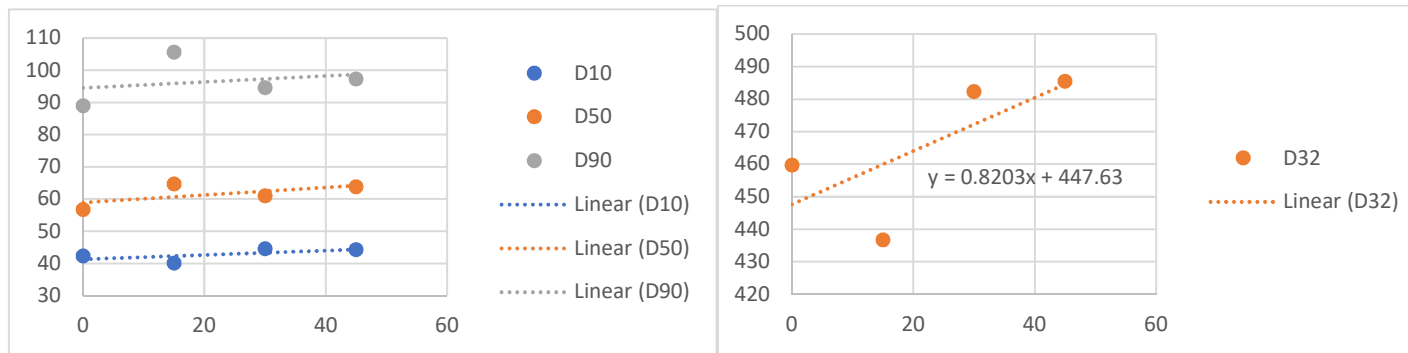
Figure 37 Re_r 15,000 Particle size graphs (D10, D50, D90, SMD)

Re$_r$ 20,000 data

Table 5 *Re*$_r$ 20,000 Particle size data

	0	1	14	16	29	31	44	46	59	61
D10	41.152	41.57	44.621	44.249	43.667	45.192	44.858	48.141	47.457	47.908
D50	56.861	55.311	62.027	62.554	63.193	63.512	66.327	67.28	70.013	68.135
D90	90.522	86.903	97.94	99.448	99.022	100.53	102.29	104.36	105.26	103.53
D43	576.57	581.33	601.51	605.94	607.36	604.81	616.39	615.11	620.84	618.18
D32	444.13	451.37	474.29	475.74	472.14	478.27	476.65	490.78	489.42	490.2

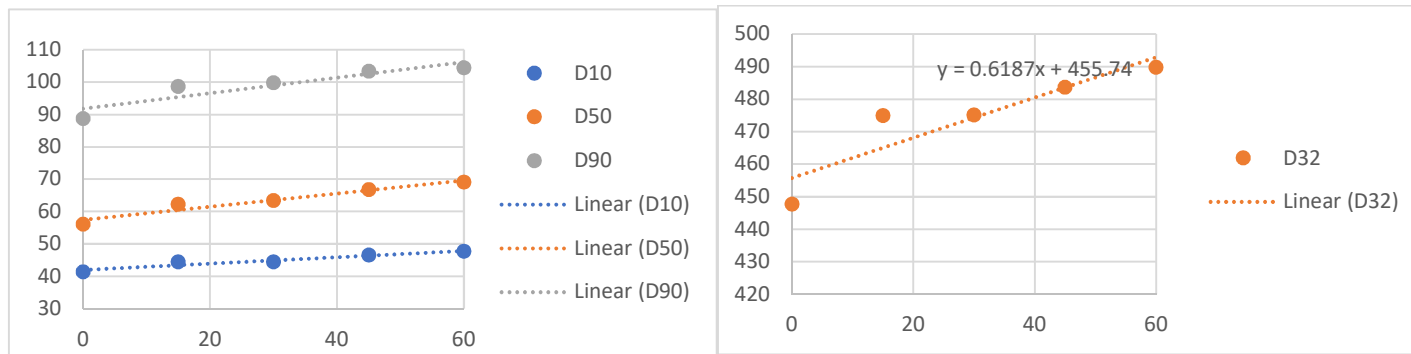Figure 38 *Re*$_r$ 20,000 Particle size graphs (D10, D50, D90, SMD)

Re_r 25,000 data

Table 6 Re_r 25,000 Particle size data

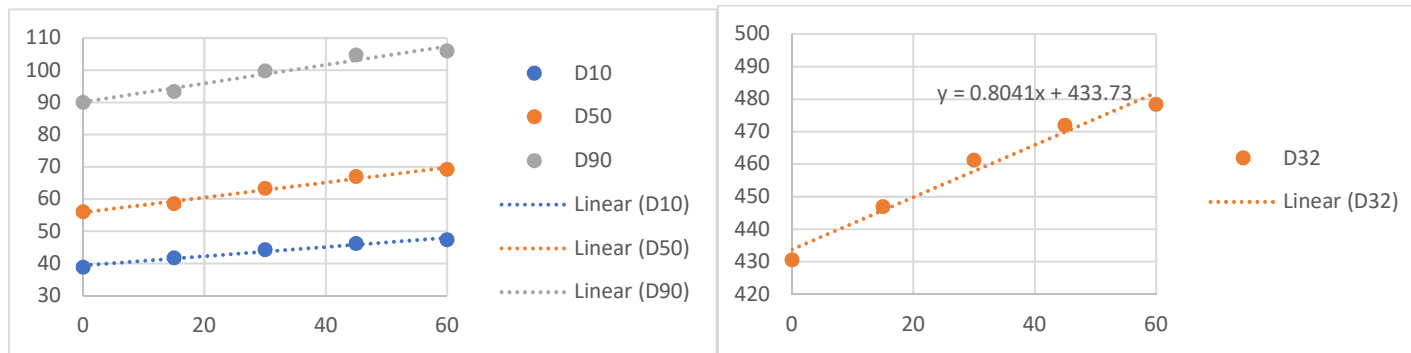|	0	1	14	16	29	31	44	46	59	61
D10	39.452	38.129	41.072	42.404	44.2	44.341	45.298	47.029	47.078	47.586
D50	56.775	55.258	58.157	58.901	64.188	62.35	66.747	67.29	69.499	68.89
D90	90.484	89.597	93.322	93.524	100.34	99.162	103.35	106.15	105.73	106.26
D43	581.6	577.88	585.78	584.2	595.49	586.74	601.04	598.59	607.44	618.06
D32	434.21	427.04	448.1	445.81	463.5	459.03	468.32	475.69	470.35	486.47

Figure 39 Re_r 25,000 Particle size graphs (D10, D50, D90, SMD)

IV

Re_r 30,000 data

Table 7 Re_r 30,000 Particle size data

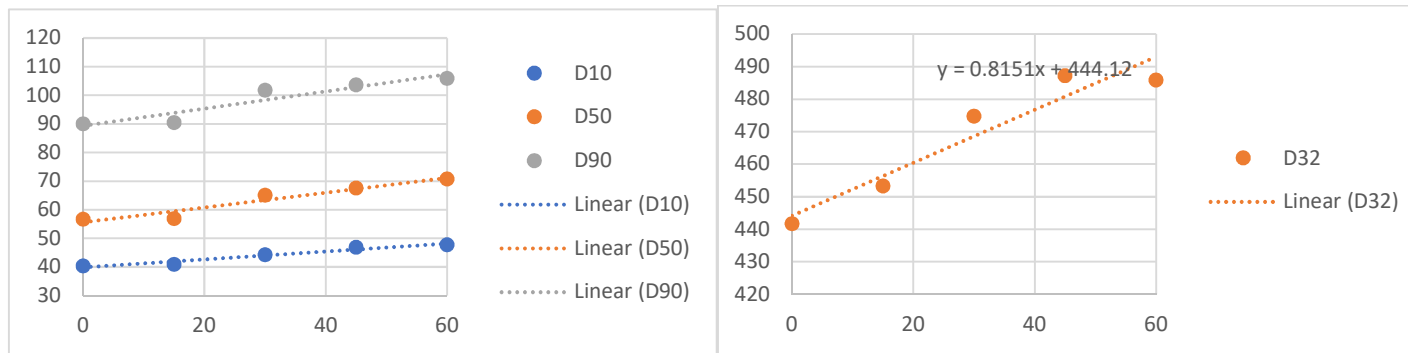|	0	1	14	16	29	31	44	46	59	61
D10	42.83	41.549	42.352	44.455	44.034	44.44	44.138	43.819	43.31	45.29
D50	59.949	58.405	61.102	61.421	62.721	60.379	63.006	60.074	61.511	61.526
D90	94.681	91.996	96.851	97.067	99.935	95.261	96.469	95.193	96.868	96.352
D43	589.7	577.72	588.18	593.47	593.48	588.45	591.9	594.49	594.79	600.87
D32	453.01	440.15	448.16	467.04	460.43	464.78	454.27	467.25	461.98	476.4

Figure 40 Re_r 30,000 Particle size graphs (D10, D50, D90, SMD)

Re$_r$ 35,000 data

Table 8 *Re$_r$* 35,000 Particle size data

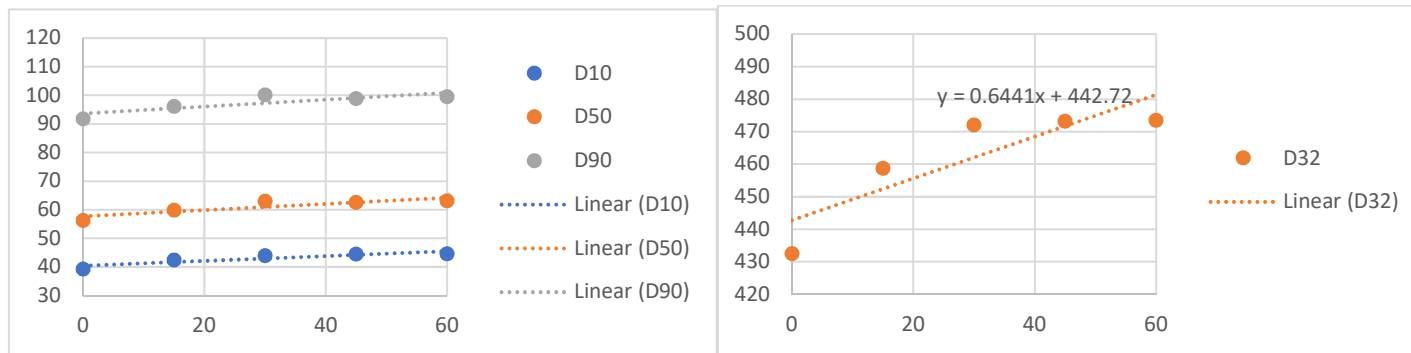|	0	1	14	16	29	31	44	46	59	61
D10	39.027	39.612	40.207	44.655	42.561	45.411	43.963	44.925	43.825	45.434
D50	56.935	55.653	56.724	62.992	62.511	63.442	62.673	62.433	62.834	63.303
D90	93.73	89.814	91.698	100.49	100.15	100.07	98.927	98.701	98.67	100.28
D43	569.84	572.59	581.58	602.79	604.23	604.79	605.9	600.36	598.73	605.02
D32	425.32	439.69	443.57	473.99	466.92	477.22	474.12	472.43	467.35	479.79

Figure 41 *Re$_r$* 35,000 Particle size graphs (D10, D50, D90, SMD)

Re$_r$ 40,000 data

Table 9 Re$_r$ 40,000 Particle size data

	0	1	14	16	29	31	44	46	59	61
D10	42.747	38.177	41.803	42.573	46.628	47.326	42.957	45.135	44.667	46.876
D50	57.074	49.095	57.969	56.902	63.269	63.869	59.53	61.719	61.614	63.574
D90	89.769	75.772	92.345	91.828	98.971	100.31	94.118	97.218	96.377	99.462
D43	590.92	548.24	583.66	587.63	601.94	603.18	595.33	598.15	597.68	616.72
D32	449.59	424.12	453.45	458.84	473.91	480.49	465.74	472.91	467.65	488.37
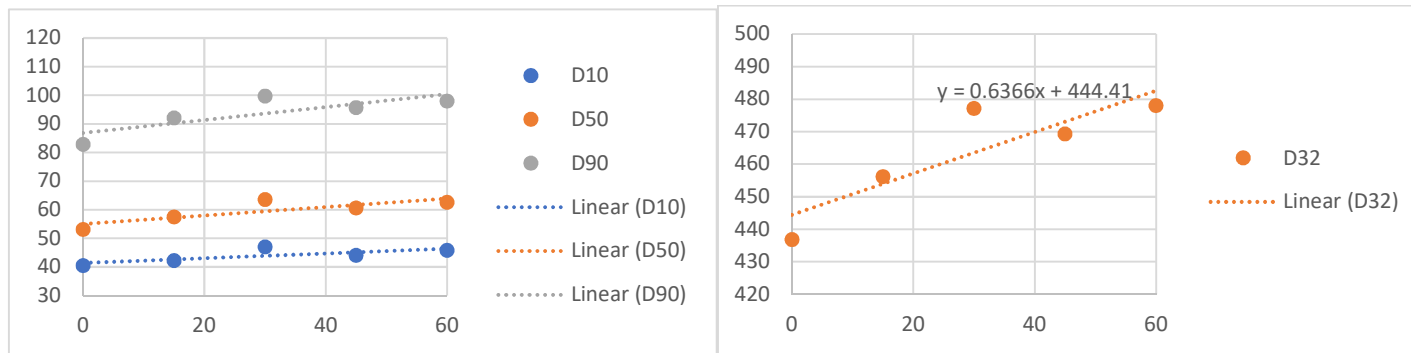
Figure 42 Re$_r$ 40,000 Particle size graphs (D10, D50, D90, SMD)

Re$_r$ 45,000 data

Table 10 *Re$_r$* 45,000 Particle size data

	0	1	14	16	29	31	44	46	59	61
D10	47.364	46.469	46.474	47.822	48.04	47.915	49.082	48.603	42.552	50.152
D50	67.851	66.104	67.088	66.954	72.06	67.762	73.475	71.709	64.161	74.008
D90	113.27	113.7	106.56	106.3	152.05	109.67	114.85	114.64	113.71	115.77
D43	569.46	570.25	586.89	599.47	552.36	593.57	598.99	583.09	548.87	599.48
D32	421.76	426.72	452.11	476.92	418	465.46	472.04	458.16	410.16	479.06
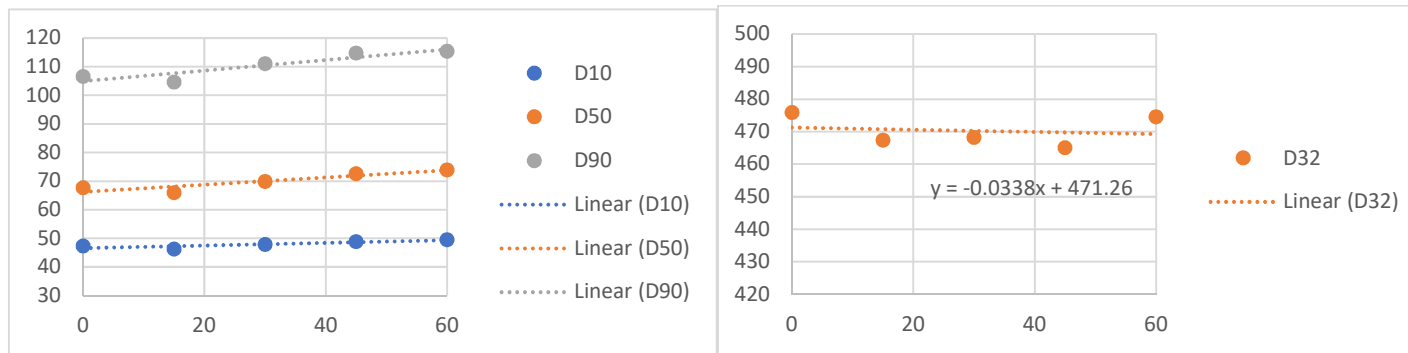
Figure 43 *Re$_r$* 45,000 Particle size graphs (D10, D50, D90, SMD)

IPF data
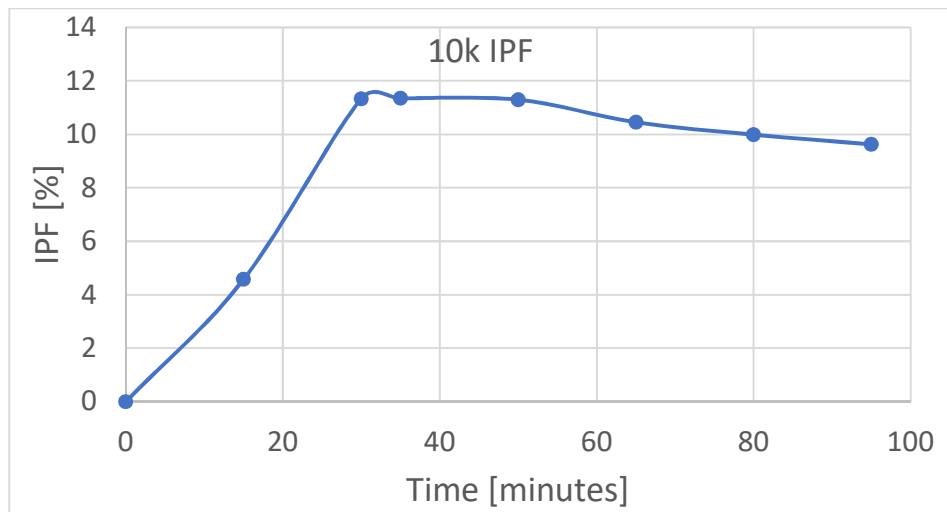
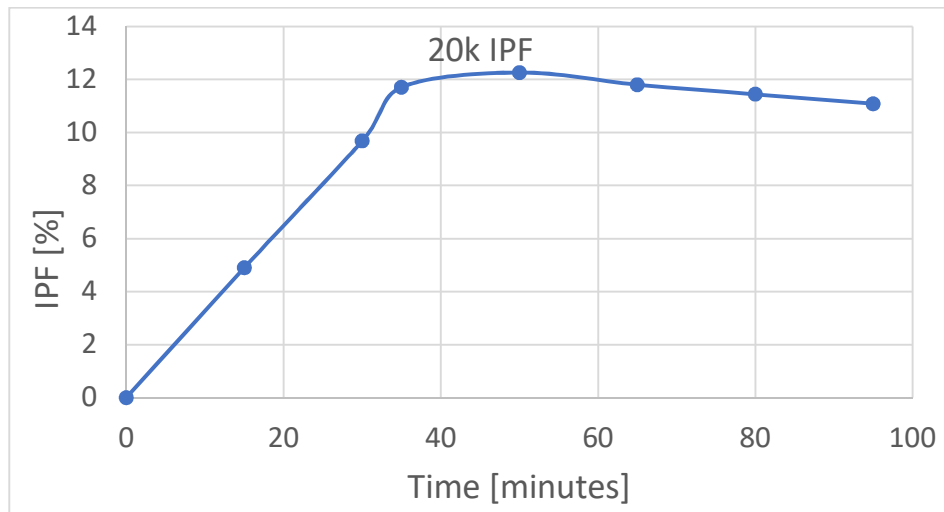Figure 44 *Re*$_r$ 10,000 IPF
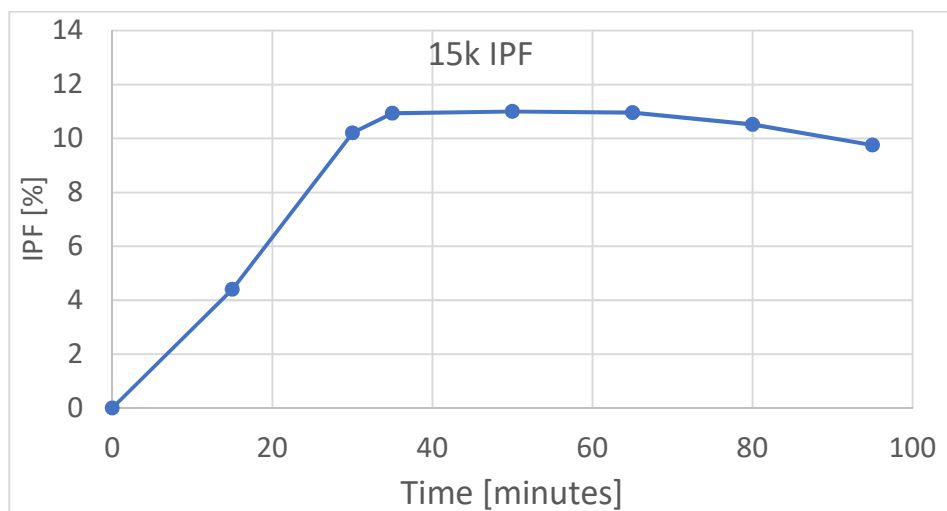
Figure 45 *Re*$_r$ 15,000 IPF
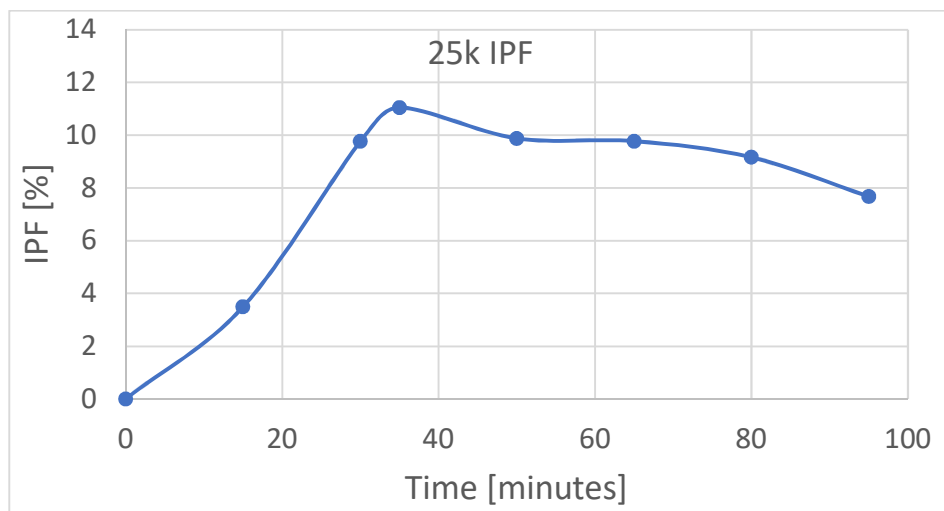
Figure 46 *Re*$_r$ 20,000 IPF
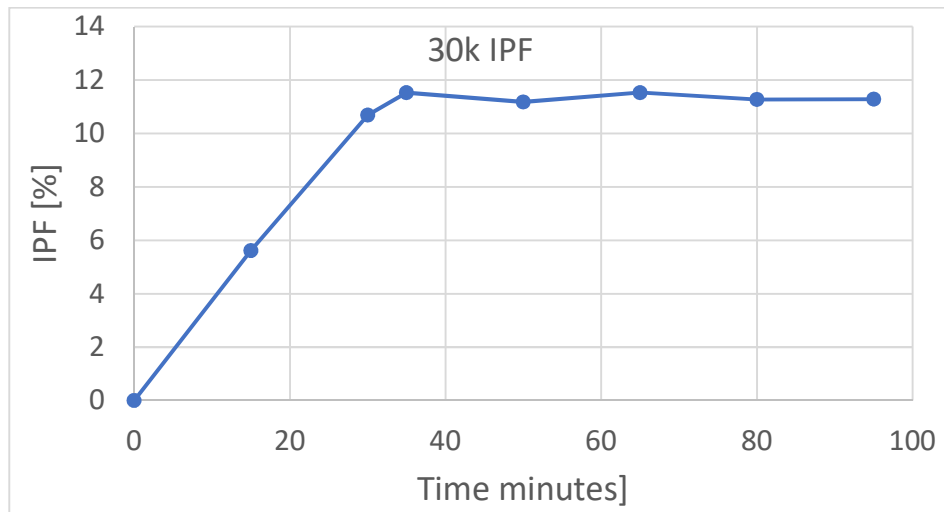

Figure 47 *Re*$_r$ 25,000 IPF

X

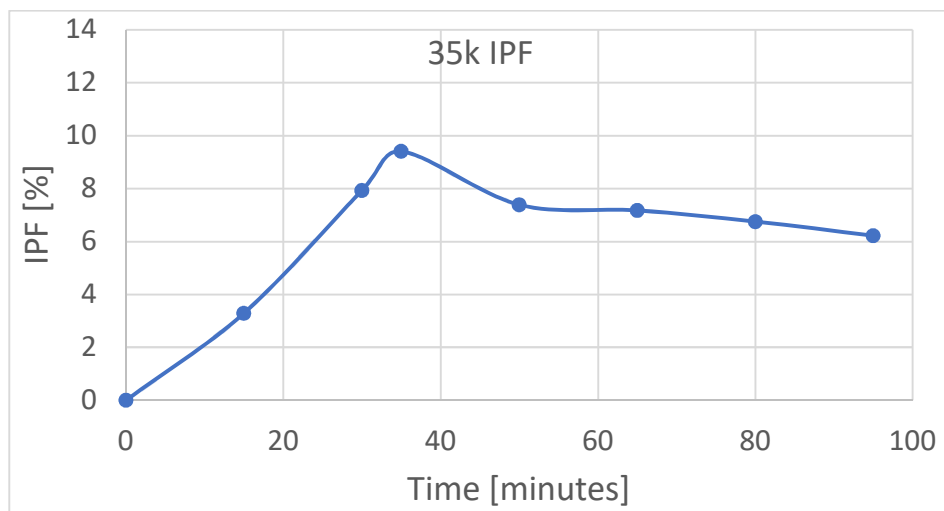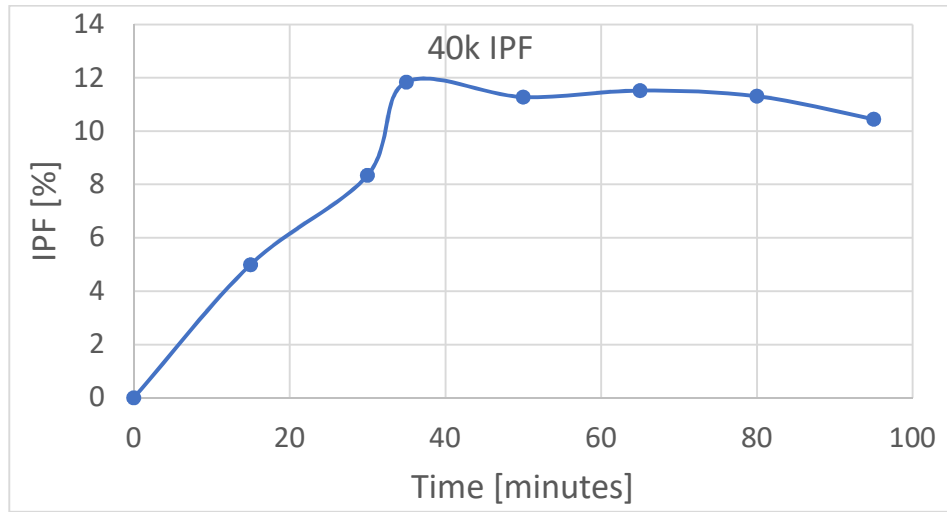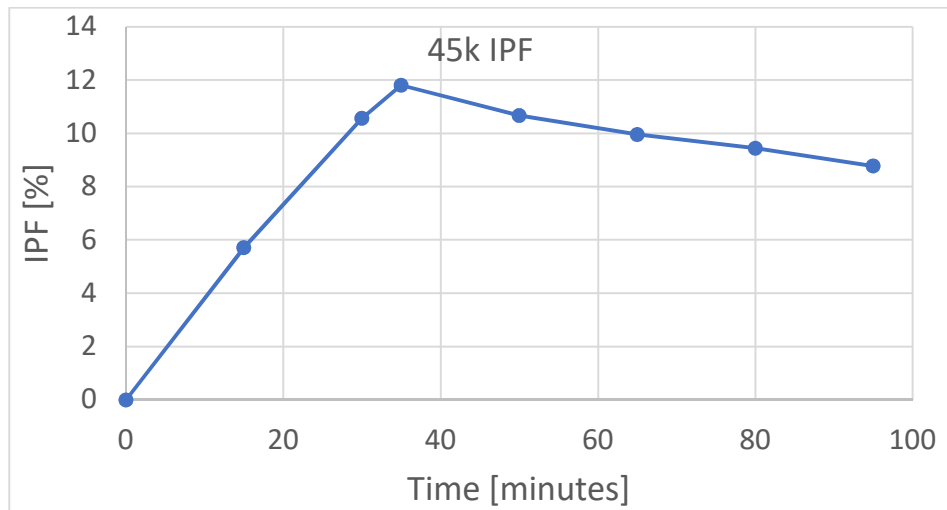Figure 48 *Re*$_r$ 30,000 IPF

Figure 49 *Re*$_r$ 35,000 IPF

XI

Figure 50 Re_r 40,000 IPF

Figure 51 Re_r 45,000 IPF